Revisiting oxygen-18 and clumped isotopes in planktic and benthic foraminifera

M. Daëron* (1) W. R. Gray (1)

* daeron@lsce.ipsl.fr

(1) *Laboratoire des Sciences du Climat et de l'Environnement, LSCE/IPSL, CEA-CNRS-UVSQ, Université Paris-Saclay, Orme des Merisiers, 91191 Gif-sur-Yvette, France.*

This is a peer-reviewed postprint submitted to EarthArXiv, currently in press at *Paleoceanography & Paleoclimatology*.

Abstract

Foraminiferal isotopes are widely used to study past oceans, with different species recording conditions at different depths. Their $\delta^{18}O$ values record both seawater oxygen-18 and temperature according to species-specific fractionation factors, while their Δ_{47} signatures likely depend only on temperature. We describe an open-source framework to collect/combine data relevant to foraminiferal isotopes, by constraining species-specific oxygen-18 fractionation factors ($^{18}\alpha$) based on culture experiments, stratified plankton tows or core-top sediments; compiling stratified plankton tow constraints on living depths for planktic species; extracting seawater temperature, $\delta^{18}O$, and chemistry from existing databases for any latitude, longitude, and depth-range; inferring calcification temperatures based on the above data. We find that although $^{18}\alpha$ differs between species, its temperature sensitivity remains indistinguishable from inorganic calcite. Based on >2600 observations we show that, although most planktic $\delta^{18}O$ values are consistent with seawater temperature and $\delta^{18}O$ over their expected living depths, a sizable minority (12–24 %) have heavier-than-predicted $\delta^{18}O$, best explained by calcification in deeper waters. We use this framework to revisit three recent Δ_{47} calibration studies of planktic/benthic foraminifera, confirming that planktic Δ_{47} varies systematically with oxygen-18-derived temperature estimates, even for samples whose $\delta^{18}O$ disagrees with assumed climatological conditions, and demonstrating excellent agreement between planktic foraminifera and modern, largely inorganic Δ_{47} calibrations. Benthic foraminifera remain ambiguous: modern benthic Δ_{47} values appear offset from planktic ones, yet applying equilibrium Δ_{47} calibration to the Cenozoic benthic foraminifer record of *Meckler et al.* (2022) largely reconciles it with $\delta^{18}O$-derived temperatures, with discrete $\Delta_{47}/\delta^{18}O$ discrepancies persisting in the Late Paleocene/Eocene/Plio-Pleistocene.

Key points

- We provide an open-source, data-driven framework to collect and combine data relevant to foraminifer isotope records.
- Δ_{47} and $\delta^{18}O$ thermometers agree well in planktics and indicate that calcification can sometimes occur below usually assumed living depths.
- Planktic Δ_{47} follows I-CDES calibrations, challenging prior Cenozoic Δ_{47} interpretations; benthics may differ and require new observations.

1 Introduction

Due to their cosmopolitan distribution, abundant preservation, and long stratigraphic record (from the Cretaceous onwards), the shells of foraminifera (typically calcitic, occasionally aragonitic) provide widely used records of past and present ocean conditions. The variety of depths preferentially inhabited by different species means that planktonic foraminifera record conditions throughout the upper water column, while benthic foraminifera provide information on the deep ocean. Such foraminiferal records underlie much of our understanding of past climate change (e.g., *Hansen et al.*, 2013; *Tierney et al.*, 2020; *Westerhold et al.*, 2020).

Methods to reconstruct past ocean conditions are based on both foraminiferal assemblages and an ever expanding array of elemental and isotopic signals measurable in their shells (see *Schiebel et al.*, 2018, for a recent review). The ratio of oxygen-18 to oxygen-16 in $CaCO_3$ ($\delta^{18}O_c$) is one of the oldest and most widely applied geochemical proxies for temperature (*Urey*, 1947; *Epstein et al.*, 1953), and the benthic $\delta^{18}O$ record captures orbital scale variability that can be precisely replicated in cores from multiple ocean basins extending back 66 Ma (e.g., *Westerhold et al.*, 2020, and references therein). However, foraminiferal $\delta^{18}O$ reflects a combination of both the local temperature and the local oxygen-18 composition of seawater ($\delta^{18}O_{sw}$) at the time of calcification, the latter term reflecting both regional hydrography and secular changes in global ice volume (e.g., *Shackleton*, 1967). Furthermore, a variety of relationships, some of them species-specific, have been proposed to describe the temperature-driven fractionation of oxygen isotopes in foraminiferal calcite (e.g., *Shackleton*, 1974; *Marchitto et al.*, 2014), and oxygen-18 fractionation also appears sensitive to seawater carbonate chemistry (*Spero et al.*, 1997; *Zeebe et al.*, 2008) as well as the intensity of light in symbiont-bearing species (*Spero*, 1992; *Spero & Lea*, 1993; *Bemis et al.*, 1998). Historically, these effects have often been labeled, somewhat indiscriminately, as "vital effects" and are implicitly or explicitly interpreted as biochemically induced deviations from isotopic equilibrium. For planktic foraminifera, further complication comes from the fact that the link between their calcification temperatures — which may vary with depth and season — and mean annual sea surface temperatures (or some other convenient metric used to describe the climate) is non-trivial and cannot be assumed to remain constant at geological timescales.

More recently, carbonate clumped-isotope (Δ_{47}) paleothermometry has allowed calcification temperature to be directly constrained, enabling both temperature and $\delta^{18}O_{sw}$ to be reconstructed from foraminiferal $CaCO_3$ (*Eiler*, 2011). Over the past two decades, clumped-isotope geochemistry has seen a steady stream of methodological improvements driven by concerted community efforts, recently leading to the definition of the I-CDES reference scale (InterCarb - Carbon Dioxide Equilibrium Scale), which resolves long-standing inter-laboratory discrepancies in carbonate Δ_{47} measurements (*Bernasconi et al.*, 2021), along with apparently unifying calibrations of calcite Δ_{47} thermometry (*Anderson et al.*, 2021). Calibration studies have so far concluded that the relationship between foraminifer calcification temperatures and their Δ_{47} values is the same as that for the majority of $CaCO_3$ minerals, including many inorganic/synthetic carbonates (*Tripati et al.*, 2010; *Grauel et al.*, 2013; *Peral et al.*, 2018; *Piasecki et al.*, 2019; *Meinicke et al.*, 2020). Although they predate the I-CDES itself, the latest three of these studies anchored their Δ_{47}

measurements to the same carbonate reference materials used to define the I-CDES scale. In theory, this should make it straightforward to directly compare their results, but as pointed out by *Meinicke et al.* (2020) there are important differences in how these studies estimate "true" calcification temperatures independently of Δ_{47}.

In this work, we start by laying out a comprehensive framework for the quantitative interpretation of oxygen-18 in foraminifera, bringing together (a) an extensive compilation of core-top and culture studies and plankton tow data constraining oxygen-18 fractionation factors as a function of temperature in different foraminiferal species, (b) a compilation of typical habitat depths for planktic species from depth-stratified tows, and (c) modern seawater temperature/$\delta^{18}O_{sw}$/chemistry databases. This framework is generally consistent with a large compilation of planktic foraminifera from Holocene core tops (*Malevich et al.*, 2019), although it raises questions regarding true calcification depths. Building on this framework, we then jointly reassess the results of the three most recent foraminifer Δ_{47} calibration studies. We find excellent agreement, as previously reported, between $\delta^{18}O$-derived and Δ_{47}-derived temperature estimates in planktic foraminifera, implying that they conform to recently published, mostly inorganic I-CDES calibrations. The case of benthic foraminifera is not as clear-cut, with conspicuous discrepancies between atlas and clumped-isotope estimates of temperature. Despite its first-order approximations and assumptions, we believe this case study showcases how the framework described here provides a useful, data-based foundation to interpret foraminiferal isotopic records. While many of the calibration issues discussed here may seem to be deep in the methodological weeds of $\delta^{18}O$ and Δ_{47} thermometry, we illustrate in the final section how these issues, and the related uncertainties, have a far from trivial impact on our understanding of Cenozoic climate evolution, and by inference of climate sensitivity and polar amplification derived from these records (*Hansen et al.*, 2013; *Cramwinckel et al.*, 2018; *Westerhold et al.*, 2020; *Gaskell et al.*, 2022).

2 Objectives and Methods

2.1 Objectives

Paleoceanographic reconstructions based on foraminiferal $\delta^{18}O_c$ are one of the oldest branches of paleoclimatology (*Emiliani*, 1954a,b). Many of the concepts and nomenclature in use today (e.g., "vital effects" or "expected equilibrium values") reflect this long history, and some of the classical formulas still routinely used are at odds with more recent, yet robust observations. This is particularly apparent when combining oxygen-18 methods with other tracers of seawater temperature, such as Mg/Ca ratios (*Weldeab et al.*, 2007) or clumped isotopes (*Meckler et al.*, 2022), each with their own set of methodological challenges. This work aims to revisit the consistency between climatological, $\delta^{18}O$, and Δ_{47}-derived temperatures, with our primary targets being (1) to critically revisit the methods by which we may use oxygen-18 thermometry to constrain foraminiferal calcification temperatures, and (2) to reassess, based on the overall I-CDES-reprocessed clumped-isotope data set, whether the Δ_{47} values of foraminifera differ significantly from those predicted by I-CDES calibration studies based on other types of biogenic or abiotic carbonates (*Anderson et al.*, 2021; *Fiebig et al.*, 2021).

2.2 Least-squares methods

Regression methods used in this study are either "simple regressions", i.e. least-squares regression only considering residuals in the dependent variable, with each observation carrying an equal weight and no attempt to quantify model uncertainties, or "York regressions", i.e. straight-line fitting of (X, Y) data considering uncertainties in both variables (*York et al.*, 2004). In the latter case, we use the root mean squared weighted deviation statistic (RMSWD), equivalent to the square root of the reduced χ^2 statistic, to assess goodness-of-fit:

$$\mathrm{RMSWD} = \sqrt{\chi^2 / N_f} \qquad N_f \text{ being the number of degrees of freedom} \tag{1}$$

As a rule of thumb, RMSWD values can be used to check *a posteriori*, based on the magnitude of the regression residuals, whether observation uncertainties have been reasonably assigned: a RMSWD value much larger than one suggests that the uncertainties assigned to the (X, Y) observations are underestimated by a factor roughly equal to the RMSWD value. Conversely, a RMSWD value much less than one is suggestive of overestimated uncertainties.

2.3 Clumped-isotope data sets

2.3.1 Original studies

Peral et al. (2018) analyzed 25 planktic and 2 benthic foraminifer samples from 12 core tops (table 1; fig. 1). Samples in that study were reacted in a common acid bath at 90 °C and the typical amount of $CaCO_3$ per replicate analysis was 20 –30 μmol. They did not find evidence for detectable size fraction effects on Δ_{47} nor $\delta^{18}O$, except for *G. inflata* whose carbonate $\delta^{18}O$ values ($\delta^{18}O_c$) varied substantially ($\pm$0.4 ‰) with size fraction. Different size fractions for *G. inflata* were thus treated as independent samples (using the nomenclature of *Daëron* (2021), where *sample*

designates some amount of homogeneous carbonate material subjected to one or more replicate *analyses*), while samples for the other species were defined as a unique combination of core-top and species. The *Peral et al.* results are consistent with earlier evidence (*Tripati et al.*, 2010; *Grauel et al.*, 2013) arguing against large species-specific or pH-dependent effects on foraminifer Δ_{47}.

Piasecki et al. (2019) and *Meinicke et al.* (2020) both used another sample preparation protocol, where smaller replicates (each ∼1.0 –1.5 μmol) were acid-reacted at 70 °C using a modified Kiel device. *Piasecki et al.* analyzed 43 benthic samples from 13 core tops. They did not find evidence for detectable species or size fraction effects on Δ_{47}, and thus computed the average Δ_{47} composition for each of the 13 core tops by binning all size fractions and all species together at each site. *Meinicke et al.* analyzed 43 planktic samples from a different set of 13 core tops. They did not specifically test for size effects on Δ_{47}, but again concluded against detectable species-specific effects.

Peral et al. and *Meinicke et al.* tested various methods aiming to estimate "true" planktic calcification temperatures independently of Δ_{47}. These methods can be broadly categorized as either based on seawater atlas temperatures or based on oxygen-18 thermometry. In the first case, calcification temperatures are constrained by looking up, in a gridded database such as the World Ocean Atlas (WOA) (*Locarnini et al.*, 2018), monthly or seasonally averaged seawater temperatures corresponding jointly to a certain seasonal time window and a certain range of water depth. These space-time constraints are assigned *a priori* and depend on the planktic species considered. The second approach, instead of seawater temperatures, considers seawater $\delta^{18}O$ values ($\delta^{18}O_{sw}$) based on a gridded database of mean annual $\delta^{18}O_{sw}$ (*LeGrande & Schmidt*, 2006) and combines this information with foraminifer $\delta^{18}O$ measurements to constrain calcification temperatures.

Despite using slightly different methods to estimate calcification depths, both *Peral et al.* and *Meinicke et al.* concluded that temperature estimates obtained from the isotopic method are more useful, largely because of strong seasonal variations in seawater surface temperatures (SST) whereas $\delta^{18}O_{sw}$ remains relatively constant within the water column and throughout the year. However, the two groups ended up making different choices regarding which water-calcite oxygen-18 fractionation relationship best applies to planktic foraminifers. *Peral et al.* opted for the *Kim & O'Neil* (1997) calibration, which is based on synthetic calcites precipitated at 10 °C, 25 °C and 40 °C. They argued that this assumption, when combined with seawater temperature databases and models of temperature-dependent foraminifer calcification rates based on culture experiments (*Lombard et al.*, 2009), yields good first-order predictions for foraminifer $\delta^{18}O_c$ values, with root mean square residuals on the order of 0.2 ‰ (*Roche et al.*, 2018). Conversely, *Meinicke et al.* opted for the calibration of *Shackleton* (1974, eq. D), which is derived from synthetic calcites precipitated at 0 °C and 25 °C (*O'Neil et al.*, 1969; *Tarutani et al.*, 1969) and was found to be consistent with benthic *Uvigerina* from three core tops with modern temperatures between 1 °C and 7 °C. The effect of choosing the former calibration over the latter is negligible at ∼20 °C, but reaches +1.5 °C around 30 °C and −2.2 °C around 0 °C (fig. 4D of *Meinicke et al.*, 2020).

All of the benthic foraminifera analyzed by *Peral et al.* and *Piasecki et al.* were collected from core tops, in sediments younger than 6 ka. *Piasecki et al.* assigned benthic calcification temperatures based either on *in situ* measurements reported in earlier studies or on WOA estimates of bottom seawater temperatures. *Peral et al.*, arguing that their 4–6 ka core-top sediments might potentially record temperatures cooler than modern ones, opted instead for oxygen-18-based estimates using the *Kim & O'Neil* (1997) calibration for *Cibicides wuellerstorfi* and the same equation, modified by 0.47 ‰ after *Marchitto et al.* (2014), for *Uvigerina mediterranea*, yielding temperatures 0.7–1.2 °C lower than WOA estimates.

The findings of all three studies are summarized in fig. 2. Despite the use of different analytical protocols, these results were all anchored to the CDES scale of *Dennis et al.* (2011) using the same set of reference materials (ETH-1/2/3/4, with nominal values from *Bernasconi et al.*, 2018). However, the spread of Δ_{47} values predicted by each study at low temperature (~ 0 °C) is on the order of 18 ppm, equivalent to ~ 4 °C. Some of that spread may arise from the use of different calcification temperature assumptions, or even simply reflect analytical scatter, but it is also possible that some foraminifer groups — e.g., benthic vs planktic — are characterized by different relationships between Δ_{47} and temperature.

2.3.2 Conversion to Δ_{47} (I-CDES) values

We reprocessed the original raw data of *Peral et al.* using a "pooled regression" approach as implemented by the `D47crunch` library (*Daëron*, 2021), using the I-CDES nominal values assigned to ETH-1/2/3/4 by *Bernasconi et al.* (2021). As in the original study, "samples" are defined by default as a unique combination of core site, species, and size fraction. We then use `D47crunch`'s built-in `combine_samples()` method to combine all size fractions with the same core and species, except for *G. inflata* samples (see section 2.3.1). By properly accounting for analytical error covariance between the Δ_{47} values to combine, this two-step approach avoids underestimating the final standardization errors.

The original data of *Meinicke et al.* (2020) were reprocessed by *Meinicke et al.* (2021) who provided a recalculated I-CDES calibration equation. Although the corresponding raw data are archived in the EarthChem database, the Kiel-device approach used at the University of Bergen standardizes measurements based on reference materials analyzed in a sliding time window rather than grouping analyses in discrete analytical sessions. Despite this approach being entirely valid in itself, the statistical treatment implemented in `D47crunch` does not properly apply in the case of a sliding window, and to the best of our knowledge there is no published method to reliably propagate full standardization uncertainties for that approach. However, when following best practices (replicate analyses sufficiently separated in time; evenly distributed measurements of standards) the sliding window approach should provide useful estimates of analytical repeatability despite effectively neglecting all inter-sample error correlations. Instead of attempting to reprocess the original data of *Piasecki et al.* and *Meinicke et al.* ourselves, we thus opted to use reprocessed Δ_{47} (I-CDES) sample mean values kindly provided by N. Meckler and N. Meinicke.

Full analytical Δ_{47} uncertainties for the *Peral et al.* data are provided directly by `D47crunch` reprocessing. For each of the two other studies, we determine the pooled external Δ_{47} repeatability at the replicate level for all unknown samples (0.032 ‰ and 0.033 ‰ for *Piasecki et al.* and *Meinicke et al.*, respectively), and approximate the mean Δ_{47} uncertainty for each sample by dividing this value by the square root of the number of replicates for this sample.

2.4 Estimates of calcification temperatures from the World Ocean Atlas

We model bottom seawater temperatures at a given latitude, longitude and depth by interpolating the gridded mean annual temperature field from the WOA 2023 Temperature Climate Normals (https://www.ncei.noaa.gov/products/world-ocean-atlas). For some sites near coastlines, interpolated values do not extend down to the true depth of the core-top. In such cases, we estimate bottom seawater temperature at the core top by using the nearest neighboring grid node with a temperature profile reaching sufficient depth. We check the consistency between the temperature profile interpolated at the latitude and longitude of the core and the nearest-neighbor temperatures by visual inspection of the two superimposed profiles (supplemental fig. S1).

For seawater temperatures nearer to the surface, which potentially experience large seasonal variations, at a given latitude and longitude we interpolate the gridded mean monthly temperature fields from the same WOA23 database. This allows us to compile, for any given site, histograms of temperatures integrated over arbitrary ranges of calcification depths and months.

2.5 Estimates of calcification temperatures from oxygen-18

2.5.1 Species-specific oxygen-18 fractionation relationships

As previously argued by *Peral et al.* and *Meinicke et al.*, we concur that oxygen-18 thermometry potentially provides reasonably accurate constraints on planktic foraminifer calcification temperatures, but with an important caveat: that such estimates are critically sensitive to the decision of which oxygen-18 fractionation relationship(s) should apply. Here, we address this issue through the pragmatic approach of compiling published data reporting $^{18}O/^{16}O$ fractionation between seawater and foraminifera at various temperatures, either from culture experiments, from stratified plankton tows, or from sediment samples in the case of benthic species (table 2). This compilation only includes studies with direct temperature measurements and direct $\delta^{18}O_c$ and $\delta^{18}O_{sw}$ measurements which can be linked reasonably well to the modern VPDB and VSMOW scales. We excluded several studies in which there were only a few observations spanning a narrow range of temperature, but in which the oxygen-18 dispersion was unrealistically large (much greater than ±1 ‰). As noted by *Mulitza et al.* (2003), their tow results for *T. sacculifer* differ from earlier culture experiments (*Erez & Luz*, 1983; *Spero & Lea*, 1993), perhaps due to differences in carbonate chemistry between the culture experiments and the present-day ocean. We thus elected to exclude *T. sacculifer* observations from these earlier culture studies. Finally, for one of the stratified plankton tow studies, that of *Lončarić et al.* (2006), we applied an additional data filter by only considering collection depths consistent with our best estimates for the living depths of *G. inflata* and *G. truncatulinoides* (see section 2.5.2).

2.5.2 Estimates of calcification depth and seawater $\delta^{18}O$

For each species of planktic foraminifera, we compiled typical living depths based exclusively on previously published estimates from depth-stratified plankton tow hauls (*Rebotim et al.*, 2017; *Meilland et al.*, 2019; *Greco et al.*, 2019). Although true calcification depths may in theory differ from habitat depth, and both are likely to vary geographically, seasonally, and at longer, geologic timescales, we make the pragmatic initial assumption that planktic foraminifera may calcify at any depth within the generally assumed habitat range listed in table 3. We acknowledge that this assumption is far from robust when attempting to derive calcification conditions from *temperature* profiles, due to potentially strong vertical gradients and/or seasonal variations in SST. However local $\delta^{18}O_{sw}$ values, by contrast, are much more constant as a function of season and/or depth, with typical residuals of ±0.11 ‰, roughly equivalent to ±0.6 °C (see fig. 4A).

Here, instead of the seawater $\delta^{18}O$ model of *LeGrande & Schmidt* (2006), we use the gridded model of monthly averaged $\delta^{18}O_{sw}$ by *Breitkreuz et al.* (2018), which is derived from the same $\delta^{18}O$ observations as *LeGrande & Schmidt*, but combines them with a general circulation model and additional climatological observations of temperature and salinity. This approach avoids sharp transitions between water masses or in areas with sparse observations, and takes seasonal variability into account in a manner consistent with physical laws, yielding monthly as well as annual mean values of $\delta^{18}O_{sw}$ with a grid resolution of one degree. To produce monthly average $\delta^{18}O_{sw}$ profiles at a given latitude and longitude, we use the same method as for temperature profiles (section 2.4), by looking for the nearest neighboring grid node with sufficient depth range.

Given any combination of latitude, longitude, and planktic foraminifer species, we start by looking up the minimum and maximum living depths for that species (table 3). We then select the nearest grid node with sufficient depth range, and interpolate each monthly mean $\delta^{18}O_{sw}$ profile over the living depth range with a depth resolution of 1 m. Over a depth range of N meters, this process yields population of $(N + 1) \times 12$ values, whose arithmetic mean provides an estimate of $\delta^{18}O_{sw}$ for this particular combination of latitude, longitude, and species. The standard deviation of this population, noted σ_{ssv}, is used to quantify the spatial and seasonal variability of $\delta^{18}O_{sw}$ in the model. The final standard error assigned to $\delta^{18}O_{sw}$ for this particular combination of latitude, longitude, and species is defined as the quadratic sum of σ_{ssv} (reflecting in-model variability at this site) and an arbitrary "model error" of 0.1 ‰ reflecting the model's accuracy.

2.5.3 Isotopic estimates of calcification temperature

For all benthic and planktic samples in the three Δ_{47} studies, we compute "oxygen-18" estimates of temperature (T_{18}) by combining (1) $\delta^{18}O_c$ values originally reported for that sample, (2) $\delta^{18}O_{sw}$ values estimated as in section 2.5.2, (3) a species-specific relationship linking temperature to the oxygen-18 fractionation factor $^{18}\alpha$ between carbonate and water. In some cases where we lack observations constraining $^{18}\alpha$ for a given species, we use an aggregate relationship derived from observations on other species of the same genus. In the single case of *Pulleniatina*

obliquiloculata, lacking observations at the genus level, we resort to an even more generalized relationship based on aggregating all planktic species. Although this issue with *P. obliquiloculata* only affects 3 out of 68 planktic samples, it remains potentially problematic (cf further discussion in section 3.4.3).

The uncertainty associated with each T_{18} value is computed as the quadratic sum of three independent error components derived respectively from (1) the final standard error on $\delta^{18}O_{sw}$ as defined in section 2.5.2, (2) the reported standard error on $\delta^{18}O_c$, (3) the uncertainty on the species-specific relationship linking temperature to $^{18}\alpha$.

3 Results & Discussion

3.1 Species-specific oxygen-18 fractionation relationships

Figure 3 shows oxygen-18 fractionation observations for the studies listed in table 2. In spite of clear species-specific offsets, for all species with sufficient temperature coverage the thermal sensitivity of $^{18}\alpha$ is very close to the *Kim & O'Neil* (1997) slope of –0.2 ‰ per K, which is itself indistinguishable from that for quasi-equilibrium $^{18}\alpha$ values (*Daëron et al.*, 2019) or for dissolved carbonate/water and bicarbonate/water fractionations (*Beck et al.*, 2005). These observations may be simply explained by postulating that, to the first order, the temperature sensitivity of $^{18}\alpha$ is inherited from dissolved (bi)carbonate ions, with additional, second-order non-equilibrium fractionation effects controlled by other factors such as pH, ion concentrations or symbiont activity.

As a practical course of action, we propose to approximate $^{18}\alpha$ for each species as an affine function of the form $1000 \cdot \ln(^{18}\alpha) = A/T + B$, with $A = 18.03 \cdot 10^3$ after *Kim & O'Neil* (1997) and B being a species-specific offset, determined by least-squares regression of the data shown in fig. 3. We acknowledge that this approximation fails to account for the influence of factors other than temperature, such as for instance the indisputable effects of lighting conditions on $^{18}\alpha$ values in *O. universa* (fig. 1 of *Bemis et al.*, 1998). These second-order factors, however, are also sampled in the data set compiled here (for example, both high- and low-light *O. universa* experiments are included in fig. 3). We can thus estimate the scatter introduced by non-thermal factors based on the regression residuals for each species. A histogram of all such residuals is shown in fig. 4B, with 95 % of the residuals within ±0.42 ‰, roughly equivalent to ±2 °C. To the best of our knowledge, none of the existing methods for reconstructing environmental paleotemperatures offer much better precision/accuracy than that, particularly when considering that these residuals of ±0.42 ‰ reflect a combination of the natural, "true" variability of foraminiferal oxygen-18 thermometry with observation errors in temperature estimates, $\delta^{18}O_{sw}$, and $\delta^{18}O_c$ measurements. These observation errors are likely to cancel out for regressions based on many observations such as those of fig. 3, so that the accuracy of temperature reconstructions derived from sufficiently precise constraints on $\delta^{18}O_{sw}$ and $\delta^{18}O_c$ may end up being better than ±2 °C.

We thus propose that the first-order species-specific oxygen-18 fractionation relationships summarized in table 4 and fig. 5 provide a useful, updated framework for applying oxygen-18 thermometry to foraminifer shells. This comes with the caveat, however, that there are still

many gaps in our understanding of non-equilibrium fractionation effects in foraminifer shells (and, more generally, in most biogenic carbonates). As a result, predicting whether modern species-specific $^{18}\alpha$ calibrations apply to extinct species, or to past environments with a seawater chemistry very different from modern conditions, remains problematic.

3.2 Oxygen-18 estimates of planktic calcification temperatures

3.2.1 Apparent discrepancies between oxygen-18 and atlas temperatures

We assess the accuracy of our oxygen-18 estimates of calcification temperature by comparing T_{18}, for each sample, to the local temperature histogram including all monthly means over the assumed depth range for the sample's species. Most of the planktic samples in our Δ_{47} data set (52 out of 68) pass this test, but the remaining 16 "discordant" samples yield significantly cooler T_{18} values than the coldest environmental conditions (figs. 6 and 7). If we reprocess these 16 discordant samples with less strict assumptions about their calcification environment, allowing for a calcification depth range of 0–500 m, only 6 samples remain discordant.

As an independent check, we also applied the same methodology to a larger, global compilation of ∼2600 samples from core-tops (*Malevich et al.*, 2019), comprising five widely-studied planktic species (*G. ruber*, *T. sacculifer*, *G. bulloides*, *N. incompta*, and *N. pachyderma*). About 12 % of the *Malevich et al.* samples present as discordant (down to 8 % assuming 0–500 m calcification depth range), suggesting that the abundance of discordant samples in our clumped-isotope data set is not particularly unusual.

There are several possible explanations for the observation that a minority of planktic samples have oxygen-18 compositions seemingly irreconcilable with modern environmental temperatures at shallow depths:

- **Pre-Holocene foraminifera:** due to bioturbation effects, low sedimentation rates and/or poor chronological constraints, some samples may include material from glacial periods. This would be consistent with the observation that virtually all discordant samples appear cooler than expected (fig. 8), which in this scenario could result from a combination of cooler seawater and greater $\delta^{18}O_{sw}$ values in glacial times. A first-order prediction for this hypothesis is that the clumped-isotope signatures of discordant samples should accurately record the cooler waters but fail to account for the underestimated $\delta^{18}O_{sw}$, yielding Δ_{47} values greater than expected from $^{18}\alpha$ by up to ∼15 ppm (equivalent to −5 °C i.e. +1 ‰ $\delta^{18}O_{sw}$). As discussed in section 3.4.2, this does not appear to be the case.
- **Inaccurate species-specific $^{18}\alpha$ functions:** it is possible that the observations summarized in fig. 3 fail to capture the natural range of $^{18}\alpha$ values associated with some planktic species. However, the discordant observations appear to be broadly distributed among species, including some for which existing constraints on $^{18}\alpha$ seem quite robust (*G. bulloides*, *G. ruber white*).

- **Inaccurate $\delta^{18}O_{sw}$ model:** as noted by *Breitkreuz et al.* (2018), their model does not account for oxygen-18-depleted precipitation, leading to comparatively large errors in shallow Arctic seawater, at latitudes $>70\,°N$ (fig. 2 of *Breitkreuz et al.*). However, out of the 37 cores considered here, the 4 located in areas where the $\delta^{18}O_{sw}$ model performs poorly contain none of the discordant observations, which in fact appear fairly randomly distributed with respect to latitude, depth, or ocean basins. More generally, errors in $\delta^{18}O_{sw}$ are expected to equally bias all species from a given core, which is not the case.
- **Gametogenic calcite and/or deeper-than-assumed calcification:** Many planktic species are known to precipitate a layer of gametogenic calcite at depths greater than their observed living habitat. Such precipitation, taking place in deeper and colder waters, should drive $\delta^{18}O_c$ to heavier than expected values (e.g., *Duplessy et al.*, 1981; *Caron et al.*, 1990; *Spero & Lea*, 1993; *Hamilton et al.*, 2008). This explanation would be consistent with the observation that almost all of our discordant samples become concordant when relaxing calcification depth assumptions. A first-order prediction for this hypothesis is that clumped-isotope signatures should covary with T_{18} in the same way for concordant and discordant samples alike, which is indeed what we observe in section 3.4.2. Further support for that hypothesis comes from the carbon-13 composition of discordant versus concordant samples: in ocean basins with strong vertical $\delta^{13}C$ gradients (Indian and Pacific oceans), discordant samples have lower $\delta^{13}C$ values than concordant ones from the same site, whereas discordants from the North Atlantic ocean, where the gradient is much weaker, have $\delta^{13}C$ values indistinguishable from concordant samples from the same site (fig. S4). We note that, even though it appears unlikely that gametogenic and non-gametogenic calcite would strictly follow the same $^{18}\alpha$ functions, the overall resulting enrichment is unlikely to further offset apparent temperatures by more than 1 °C.
- **Cryptic diagenesis in deeper waters:** all but one discordant sample in the Δ_{47} data set have T_{18} values cooler than surface seawater but warmer than local bottom waters. This would be consistent with cryptic, partial overprinting by secondary carbonate precipitation in early-stage diagenesis, despite the absence of clear evidence for such (re)crystallization. Although it has been proposed, somewhat controversially, that burial-induced isotopic re-equilibration widely affects $\delta^{18}O_c$ in well-preserved, glassy foraminifera in an visually undetectable manner (e.g., *Bernard et al.*, 2017; *Cisneros-Lazaro et al.*, 2022), their purported diffusion mechanism would act on much longer timescales (>1 Ma) and would be expected to erase clumped-isotope signatures several orders of magnitude more rapidly than it could substantially alter $\delta^{18}O_c$.

Our provisional conclusion is that in many cases, due to a combination of gametogenic calcite production and/or greater-than-expected vertical mobility in various planktic species, we lack reliable *a priori* knowledge regarding when and where planktic calcification occurs. We thus concur with *Peral et al.* and *Meinicke et al.* that our best option is to use oxygen-18 thermometry to estimate calcification temperatures integrated over foraminiferal life-times. A critical prediction for this approach is that T_{18} and Δ_{47} should be strongly correlated and that this covariation should be the same for concordant and discordant samples.

3.2.2 Cold end-members in the planktic data set

Currently, only three planktic samples, one *N. incompta* from the Southern Ocean in *Peral et al.* and two *N. pachyderma* from the North Atlantic in *Meinicke et al.*, effectively constrain planktic Δ_{47} below 2 °C. Technically, only one of the three is flagged as discordant, but the T_{18} estimates for all three samples are well below surface WOA23 temperature estimates (fig. 15). The discordant *N. incompta* is unusual because its T_{18} of -1.1 ± 1.0 °C is irreconcilable with the local modern bottom temperature of 2.3 ± 0.2 °C, making it very unlikely that the discrepancy could result from poorly constrained calcification depth. The two *N. pachyderma* are from a region where the $\delta^{18}O_{sw}$ model of *Breitkreuz et al.* (2018) performs poorly due to oxygen-18-depleted precipitation. However, in the high-latitude environments of these three samples, the spread of monthly temperatures throughout the whole water column remains small ($\pm$0.8 °C, 1SD), so that we can reasonably reassign calcification temperatures based on this narrow temperature range at each site (but note that this affects the two *N. pachyderma* samples only minimally, increasing temperatures by $\sim$1 °C, cf supplemental fig. S3). In the rest of this study we only consider the reassigned atlas temperatures for these three samples, keeping in mind that this approach is only applicable where vertical and seasonal variations of temperature remain small.

3.3 Independent estimates of benthic calcification temperatures

Figure 9 summarizes the currently available constraints on calcification temperatures for the benthic samples of *Piasecki et al.* and *Peral et al.* whose species or genus allows using one of the $^{18}\alpha$ calibrations listed in table 4. About half of the core-top sites in fig. 9 display some kind of discrepancy between bottom temperatures estimated from WOA23, originally reported *in situ* measurements, and/or T_{18} estimates based on one or more benthic species. Some species, such as those within the *Cibicidoides* genus, yield T_{18} estimates generally consistent with atlas and *in situ* temperatures. Other species sometimes yield T_{18} clearly at odds with atlas and *in situ* estimates, in spite of apparently robust calibration constraints on $^{18}\alpha$. The worst offenders are *H. elegans*, the only aragonitic species considered here, and *U. peregrina*, the only infaunal one. For *H. elegans*, the three warmest core tops yield T_{18} estimates systematically warmer than the other species at those sites, which could reflect a potentially steeper than assumed slope of $^{18}\alpha$ (see fig. 3). In one case, *U. peregrina* yields T_{18} 7–10 °C colder than other estimates. Although it would be tempting to attribute this to inaccurate *in situ* constraints, other studies have also reported discrepancies of this magnitude between expected and observed $\delta^{18}O$ in *U. peregrina* (*Schmiedl & Mackensen*, 2006; *McCave et al.*, 2008).

Noting that T_{18} estimates, where they deviate strongly from the others, do not display any systematic bias, we propose that the most conservative strategy for now is to stick with the originally reported *in situ* temperatures, if available, and otherwise (for both of the *Peral et al.* cores and three of the *Piasecki et al.* cores) to use bottom WOA23 temperatures. The basic observation remains, nevertheless, that in several locations the $\delta^{18}O_c$ values of different species do not appear consistent with existing modern observations on $^{18}\alpha$, unless we assume that these species somehow record different temperatures and/or $\delta^{18}O_{sw}$ values.

3.4 Δ_{47} vs temperature for planktic foraminifera

3.4.1 Existing constraints on equilibrium/inorganic I-CDES calibrations

Two recent calibration studies provide constraints on the relationship between $\Delta_{47\text{-ICDES}}$ values and carbonate formation temperatures. In the first one, *Anderson et al.* (2021) analyzed six newly obtained glacial lake carbonates, and re-analyzed at MIT thirty-five samples from earlier studies comprising natural calcites, synthetic precipitates, and experimentally heated calcites. They also reported new measurements, performed at LSCE, of mammillary calcites from Devils Hole and Laghetto Basso, whose very slow, inorganic precipitation from barely supersaturated waters offer optimal conditions for achieving isotopic equilibrium (*Coplen*, 2007; *Daëron et al.*, 2019). The calibration equation published by *Anderson et al.* (2021) was obtained by combining these new results with those of previous studies including the *Peral et al.* (2018) data (with the original calcification temperature estimates based on *Kim & O'Neil*, 1997) and the planktic data of *Meinicke et al.* (2020) (with temperatures based on *Shackleton*, 1974). Directly comparing that equation to the foraminifer data we revisit here would thus present an obvious circularity. For this reason, we compute here an "MIT calibration" corresponding to the York regression of all analyses performed at MIT, based on the I-CDES values originally reported in table S1 of *Anderson et al.* (computation included in our code repository):

$$\Delta_{47\text{-ICDES}} = 38.48 \cdot 10^3/T^2 + 0.1618 \qquad \left(\text{MIT calibration}\right) \tag{2}$$

There is no such circularity issue with the calibration study of *Fiebig et al.* (2021), which includes new measurements of the same two mammillary calcite samples along with a suite of calcites precipitated or re-equilibrated at much higher temperatures. We thus use here the published version of their calibration equation:

$$\Delta_{47\text{-ICDES}} = 1.038 \times \left(-\frac{5.897}{T} - \frac{3.521 \cdot 10^3}{T^2} + \frac{2.391 \cdot 10^7}{T^3} - \frac{3.541 \cdot 10^9}{T^4}\right) + 0.1856 \tag{3}$$

$$\left(\textit{Fiebig et al.}\ \text{calibration}\right)$$

Finally, one may also constrain equilibrium Δ_{47} values at Earth-surface conditions by combining the measurements of Devils Hole and Laghetto Basso calcite reported in these two studies, for a total of 76 replicates with an external Δ_{47} repeatability of 0.009 ‰. These independent measurements yield statistically indistinguishable values (RMSE = 2.6 ppm at the sample level), yielding the following "Devils Laghetto" equilibrium relationship:

$$\Delta_{47\text{-ICDES}} = 39.09 \cdot 10^3/T^2 + 0.1535 \qquad \left(\text{Devils Laghetto calibration}\right) \tag{4}$$

The three calibrations above do not differ significantly at ambient temperatures: their maximum spread remains smaller than ±0.4 °C between 7 and 30 °C, with eq. (3) returning temperatures increasingly lower than the two other equations from 7 to 0 °C, with the total spread reaching ±0.8 °C at 0 °C, well within the 95 % confidence bounds for any of these regressions (about ± 1.8 °C for MIT and *Fiebig et al.* and around ± 1.2 °C for Devils Laghetto).

3.4.2 Δ_{47} calibration of planktic foraminifera

As shown in figs. 10–11, $\Delta_{47\text{-ICDES}}$ values for all concordant planktic samples, when plotted against T_{18}, are in excellent agreement with all three inorganic calibrations (2–4). Within the concordant planktic data set (52 samples), the *Peral et al.* (2018) results and those of *Meinicke et al.* (2020) are statistically indistinguishable (ANCOVA p-values of 0.63 and 0.14 for slope and intercept, respectively).

Strikingly, the discordant planktic samples in both studies appear to follow the same relationship between Δ_{47} and T_{18} as concordant foraminifera. The RMSWD of 0.9 for the regression of the concordant planktic samples does not change significantly when also including discordant samples, and its value around one implies that the regression residuals are consistent with those expected from the joint uncertainties in Δ_{47} and T_{18}. This is in line with our earlier hypothesis that the discordant samples simply precipitate in deeper, colder water than we would expect based on typical habitat depths.

When including both concordant and discordant samples, the reprocessed results of *Peral et al.* and those of *Meinicke et al.* are once again statistically indistinguishable (ANCOVA p-values of 0.42 and 0.13 for slope and intercept, respectively). We may thus compute the following best-fit regression for all planktic foraminifera considered here (but see section 3.4.3 below):

$$\Delta_{47\text{-ICDES}} = 36.51 \cdot 10^3/T^2 + 0.1842 \tag{5}$$

This equation may be reformulated as a sum of two statistically independent components to simplify computing regression standard errors:

$$\Delta_{47\text{-ICDES}} = A \cdot \left(\frac{10^3}{T^2} - \frac{10^3}{T_0^2}\right) + B_0 \qquad \text{with} \qquad \begin{aligned} &T_0 \equiv 287.4 \text{ K} \\ &A = 36.51 \pm 1.41 \ (1\sigma) \\ &B_0 = 0.6262 \pm 0.0009 \ (1\sigma) \\ &\text{cov}(A, B_0) = 0 \end{aligned} \tag{6}$$

Based on these results, we conclude that the relationship between calcification temperatures and $\Delta_{47\text{-ICDES}}$ values in planktic foraminifer tests is indistinguishable from that observed for inorganic calcite precipitated from solutions with isotopically equilibrated dissolved inorganic carbon (DIC). In practice, this means that the formulas in eqs. (2–6) should all yield adequate — and statistically indistinguishable, cf fig. 11 — reconstructions of planktic foraminifer calcification temperatures. However, in view of the substantial minority of planktic foraminifera whose $\delta^{18}O$

and Δ_{47} compositions both appear to record substantially deeper calcification than usually assumed, beware that these reconstructed temperatures do not necessarily reflect surface conditions exclusively.

3.4.3 Poor constraints on $^{18}\alpha$ for P. obliquiloculata

As noted in section 2.5.3, to the best of our knowledge we lack observations usable to robustly constrain the relationship between $^{18}\alpha$ and calcification temperature in *P. obliquiloculata* or in other species of the same genus. We thus originally assigned T_{18} values for the three samples of that species based on an $^{18}\alpha$ equation averaged over all planktic observations (table 4, fig. 5). All three samples are flagged as discordant, with T_{18} estimates 5–12 °C colder than atlas temperatures (fig. 15), and all of them plot well below the overall planktic Δ_{47} regression line, with some of the lowest regression residuals in the whole data set (fig. 12). Because the *P. obliquiloculata* samples are among the warmest in our data set, assigning them grossly inaccurate calcification temperatures is likely to strongly bias regression results. Using water-column-averaged monthly atlas temperatures, as we did for the cold, high-latitude samples above, is not particularly useful because the very large resulting uncertainties essentially nullify any influence these three samples may exert. Lacking a better option, we opted to exclude the *P. obliquiloculata* observations from the regression used to compute eqs. (5-6).

3.5 Δ_{47} vs temperature for benthic foraminifera

Figure 10 also shows the average Δ_{47} values of benthic foraminifera from each core site. At face value, these 15 data points do not appear consistent with the planktic regression of eq. (5), with apparent residuals ranging from −7.5 °C to −0.6 °C. The corresponding Z-scores (the "number of SE deviation" for each residual) range from −6.4 to −0.2, and only 5 scores out of 15 lie within ±1.96, i.e. the 95 % confidence interval for a normal distribution (fig. 13). Plotting these residuals and Z-scores by species/genus, instead of averaging by core site, does not reveal any obvious correlation with genus, nor between infaunal and epifaunal species (vertical and horizontal diamonds in fig. 13, respectively). Only 24 out of these 45 Z-scores lie within ±1.96, once again making it very unlikely that the benthic residuals can be attributed to random analytical scatter. Judging from these large, systematic offsets, the results obtained by *Peral et al.* (2018) and *Piasecki et al.* (2019), if taken at face value, would appear to imply that benthic foraminifera do not follow the same relationship between Δ_{47} and temperature as their planktic cousins nor, by extension, inorganic calcites.

Although other types of biogenic carbonates, such as corals and some brachiopods, display greater-than-expected Δ_{47} values, most likely reflecting disequilibrium between water and DIC associated with CO_2 absorption (*Saenger et al.*, 2012; *Bajnai et al.*, 2020; *Davies et al.*, 2022; *Letulle et al.*, 2022), there does not appear to be any correlation, as shown in fig. 14, between the benthic residuals and the seawater chemistry at the core-top sites (e.g., salinity or calcite saturation). Alternatively, the issue of large benthic residuals could be mitigated (but not eliminated) by supposing that our planktic data set underestimates cold-end-member Δ_{47} values by $\sim$20 ppm.

Note, however, that such a large bias is unlikely to simply result from inaccurate temperature constraints, in view of the narrow range of water column temperatures for the coldest planktic samples (section 3.2.2).

By contrast with these results, older core-top studies of foraminifer Δ_{47}, predating the use of I-CDES reference materials, did not report any significant discrepancies between planktic and benthic foraminifera. *Tripati et al.* (2010), based on 24 planktic and 11 benthic foraminifer samples, did not observe any obvious difference in T-Δ_{47} relationships between planktics and benthics, but any such difference would have been difficult to observe given that there was not much overlap in calcification temperatures between the two sample groups. *Grauel et al.* (2013) only analyzed three benthic samples (*U. mediterranea* and *C. pachyderma*), whose measured Δ_{47} values are arguably 10–20 ppm greater than those of planktic samples with similar calcification temperatures, but it would be difficult to claim that this apparent offset exceeds the level of analytical uncertainty in that early study.

It is notable that all but two of the published benthic data points were analyzed in the early days of a single laboratory over a relatively short time frame. Without making unfair assumptions about the methodology used by *Piasecki et al.* (2019), it bears reminding that the standardization of raw Δ_{47} values necessarily contributes to final analytical uncertainties, and that this contribution tends to affect samples analyzed together in a correlated manner (*Daëron*, 2021). After N. Meckler, who was one of the authors of the *Piasecki et al.* study and who reviewed the present work, suggested that this particular data set may not be as robust as it would be following today's best practices, we reviewed the corresponding raw data that she kindly shared and we concur that the level of replication of unknown samples and the temporal distribution of unknown versus standard replicates in that study was not ideal, making final average Δ_{47} values potentially susceptible to substantial standardization errors. This hypothesis would also be supported, albeit circumstantially, by the much improved agreement between benthic $\delta^{18}O_c$-derived and Δ_{47}-derived Cenozoic temperatures when using our new planktic calibration (see section 3.6.2 below).

In light of all the above, we strongly advocate that new, independent studies should test whether the benthic observations we have so far, most of them from a single study, can be reproduced in different laboratories, for instance by obtaining tight constraints on foraminiferal Δ_{47} in cold waters and comparing them, as was done in fig. 10, with published, robust values for natural carbonates formed at similar temperatures, e.g., Laghetto Basso calcite, lacustrine carbonates from Lakes Joyce, Fryxell, and Vanda (*Anderson et al.*, 2021), or *A. colbecki* scallops from Petrel Island (*Huyghe et al.*, 2022).

3.6 Implications

3.6.1 Oxygen-18 fractionation between seawater and foraminifera

In the context of the times, it was natural for *Craig* (1965) and *Shackleton* (1974) to interpret observations linking $^{18}\alpha$ and temperature in terms of isotopic equilibrium, even though they were well aware, as noted by *Urey* (1947), that "whether animals lay down carbonates in equilibrium with water" remained an open question. The answer to that question has strong practical consequences, however: in the classical case where two phases achieve isotopic equilibrium through equal opposite isotopic fluxes associated with a reversible reaction, the isotopic equilibrium constant can be expressed in terms of ratios of partition functions arising from statistical mechanics and generally depends only on temperature (*Urey*, 1947; *Bigeleisen & Goeppert Mayer*, 1947). By contrast, in the case of irreversible reactions or when opposing reaction fluxes differ greatly, as when carbonates precipitate rapidly from oversaturated solutions, the effective fractionation factor between phases depends on the reaction pathway(s) and their relative rates, and may thus vary with other factors than temperature such as pH, salinity, or ion concentrations (e.g., *Watkins et al.*, 2014; *Devriendt et al.*, 2017). As pointed out previously, however, it is entirely possible for a carbonate mineral to achieve clumped-isotope equilibrium despite having "bulk" $\delta^{18}O$ and $\delta^{13}C$ values out of equilibrium with water and/or DIC in its parent solution (e.g., *Eiler*, 2011; *Watkins & Hunt*, 2015).

The observations summarized in figs. 3-5 document how $^{18}\alpha$ at a given temperature may substantially differ among different benthic and planktic foraminifer species, as known since *Duplessy et al.* (1970) and *Shackleton et al.* (1973). But it is also clear that carbonate ion concentrations and pH also affect apparent $^{18}\alpha$ values in some planktic species (*Spero et al.*, 1997), as do irradiance levels in some symbiotic species (*Spero*, 1992; *Spero & Lea*, 1993; *Bemis et al.*, 1998). Defining species-specific $^{18}\alpha$ calibrations, as was done here, is a flawed but useful shorthand, where the species label is used as an imperfect alias for a complex set of chemical and metabolic conditions which we are still struggling to model quantitatively (*Zeebe et al.*, 2008). However useful this approach may be for modern observations, it comes with the critical caveat that unless we improve our quantitative understanding of oxygen-isotope fractionation in foraminifera, we are ill-equipped to assess whether the modern, observable $^{18}\alpha$ calibrations are applicable to past oceans with very different seawater chemistry.

3.6.2 Revisiting benthic Δ_{47} records of Cenozoic seawater temperatures

Our use of species-specific $^{18}\alpha$ calibrations, instead of a single general calibration as was done previously, leads to a shift of $-1\,°C$ in temperatures reconstructed using the *Peral et al.* (2022) calibration, and of $-0.5\,°C$ to $-3\,°C$ using the *Meinicke et al.* (2021) calibration, relative to their previously published equations (fig. 11). For *Peral et al.*, the difference is mostly due to the switch from *Kim & O'Neil* (1997) to updated $^{18}\alpha$ relationships, while the *Meinicke et al.* offset reflects both the switch from *Shackleton* (1974) and the inclusion, in the original publication, of *Piasecki et al.*'s benthic data. This offset is noteworthy in the context of the recent finding, by *Meckler et al.* (2022), that clumped isotopes in benthic foraminifera from the North Atlantic appear,

based on the *Meinicke et al.* (2021) calibration under the assumption that benthic and planktic Δ_{47} follow the same calibration function, to record Paleocene to Miocene temperatures much warmer (by 2–3 °C on average, cf fig. S5) than expected from classical oxygen-18 reconstructions (in this case, *Cramer et al.*, 2011), with the discrepancy potentially resolved by accounting for poorly-constrained pH effects on benthic foraminifer $\delta^{18}O_c$.

Simply updating the Δ_{47} calibration used by *Meckler et al.* to our revised planktic calibration (eq. 5) virtually eliminates the average offset between the Δ_{47}-derived paleotemperature estimates (T_{47}), and the T_{18} values from *Cramer et al.* (figs. 16-17 and S5) and brings the results of the two methods in much closer agreement over large spans of the Cenozoic (fig. 18). This is not to dispute the validity of the pH issues raised by *Meckler et al.* and others, but this finding highlights how sensitive some interpretations may be to our choice of $^{18}\alpha$ and Δ_{47} calibrations when applied to foraminifer records (see also figs. S6–S8 using other I-CDES calibrations).

Furthermore, the overall agreement between the two benthic temperature records doesn't preclude the possibility, as argued by *Meckler et al.* (2022), that clumped isotopes reveal previously unrecognized structure in the benthic carbonate record. In order to characterize any remaining mismatch between the $\delta^{18}O_c$ and reprocessed Δ_{47} records, we compute $\Delta T_{47\text{-}18}$ (fig. 17), defined as the difference between the new T_{47} values and the T_{18} values from *Cramer et al.* (2011). We estimate $\Delta T_{47\text{-}18}$ uncertainties based on (a) the analytical uncertainties reported by *Meckler et al.*, (b) the calibration uncertainties of eq. (6), and (c) the T_{18} uncertainties reported by *Cramer et al.* In an attempt to smooth out analytical scatter, we then subject the $\Delta T_{47\text{-}18}$ time-series to a LOWESS regression (*Cleveland*, 1979; *Cleveland & Devlin*, 1988) with bandwidths ranging from 5 to 25 Ma. We estimate the 95 % confidence limits for the LOWESS curve based on a quasi-Monte Carlo simulation where we quasi-randomly generate 2^{13} versions of the $\Delta T_{47\text{-}18}$ data set, whose multivariate Gaussian scatter is able to sample the error estimates described above more efficiently than traditional Monte Carlo methods (*Roy et al.*, 2023). As shown in fig. 17, $\Delta T_{47\text{-}18}$ is not statistically different from zero (at 95 % confidence level) over most of the Cenozoic. However, there are three time intervals (whose lengths are sensitive to smoothing bandwidth) centered around 57 Ma, 50 Ma, and 39 Ma, where T_{47} is still significantly warmer than T_{18}. Although this might conceivably reflect differences in spatial sampling between the two records, these offsets could just as likely indicate that one or more assumptions underlying the use of these methods are wrong during these intervals, the two most likely culprits being $\delta^{18}O_{sw}$ reconstructions based on ice volume/composition estimates, and the assumption of constant $^{18}\alpha$ relationships through time. Although the same issue might also explain Plio-Pleisotocene values of T_{47} which appear to be significantly colder than the T_{18} estimates, this observation is quite sensitive to the choice of one Δ_{47} calibration over another, because of relatively looser constraints on equilibrium Δ_{47} for temperatures close to 0 °C. Applying the MIT calibration instead of our planktic regression would increase Pleisotocene T_{47} estimates by 1 °C, and applying a recent, more comprehensive compilation of Δ_{47} calibration data based on 104 samples with formation temperatures down to −2 °C (OGLS23 calibration, *Daëron & Vermeesch*, 2023) would increase them by 1.5 °C, bringing them much closer to Pleistocene bottom water conditions.

That being said, we acknowledge that the statistical treatment performed here remains rudimentary. In particular, we are well aware that our LOWESS procedure assumes statistically independent $\Delta T_{47\text{-}18}$ uncertainties, which leads to well-known issues when smoothing data with correlated errors (e.g., *Kohn et al.*, 2000). In light of the standardization issues mentioned in section 2.3.2, this may or may not be problematic. It will be important to determine the extent and root causes of these mismatched intervals, because the scale of the discrepancies is far from negligible: an offset exceeding 3 °C in deep seawater temperatures has strong implications for the constraints we can place on parameters such as polar amplification and the Earth's climate sensitivity using the benthic record (e.g., *Hansen et al.*, 2013; *Gaskell et al.*, 2022).

3.6.3 Clumped-isotope thermometry of planktic foraminifera

The issue of a planktic Δ_{47} calibration is more straightforward, based on (a) the agreement between *Peral et al.* and *Meinicke et al.*; (b) the agreement between concordant versus discordant samples; (c) the agreement between planktic foraminifera and the (mostly) inorganic calibration data of *Anderson et al.* (2021) and *Fiebig et al.* (2021). The clumped-isotope compositions of planktic foraminifera thus appear to offer robust constraints on their calcification temperatures. However, such reconstructions should take into account the gaps in our knowledge of true mineralization depths, even for species whose living depths appear to be well-known. Similarly, our ability to reconstruct the $\delta^{18}O_{sw}$ values of ancient oceans still critically depends on our knowledge of the laws governing oxygen-18 fractionation in different foraminiferal species, and how they may have varied through time.

4 Conclusion

Here we describe an easily extendable, open-source framework to systematically compile and combine data relevant to the interpretation of foraminiferal $\delta^{18}O_c$ and Δ_{47} records. Using the best currently available constraints, it is clear that $^{18}\alpha$ calibrations differ markedly between species, although $^{18}\alpha$ sensitivity to temperature remains indistinguishable from that of inorganic calibrations such as *Kim & O'Neil* (1997) or *Daëron et al.* (2019). We should consider these species-specific calibrations as a flawed but useful shortcut, potentially masking a complex set of chemical and metabolic processes which may vary through time. Based on a large number of observations, the $\delta^{18}O_c$ values of most planktic samples are consistent with seawater temperature and $\delta^{18}O_{sw}$ over their expected living depth range. However a non-negligible proportion have heavier than predicted $\delta^{18}O_c$ values best explained by calcification in deeper, colder waters, highlighting the limits of our *a priori* knowledge of when and where planktic calcification occurs.

Based on these newly compiled $^{18}\alpha$ observations, we also revisit the assignment of oxygen-18-based calcification temperatures for the data reported by *Peral et al.* and *Meinicke et al.*. We find that Δ_{47} of planktic foraminifera in these two studies are in excellent agreement with the largely inorganic I-CDES calibrations of *Anderson et al.* (2021) and *Fiebig et al.* (2021). The benthic data reprocessed here is more ambiguous, however. On one hand, the available modern benthic observations yield apparent Δ_{47}-based temperatures colder by up to 7.5 °C than local bottom

seawater; on the other, applying an equilibrium Δ_{47} calibration to the benthic samples of *Meckler et al.* (2022) reconciles their results to the first order with the deep ocean temperature record from benthic $\delta^{18}O_c$ over most of the Cenozoic, highlighting how sensitive some interpretations may be to our choice of $^{18}\alpha$ and Δ_{47} calibrations. This apparent contradiction may be readily explained by methodological limitations in one of the modern benthic studies, but conclusively proving that this is the case will require new Δ_{47} measurements of benthic foraminifera from well-constrained core tops. Nevertheless, deep ocean temperatures derived from Δ_{47} and $\delta^{18}O$ appear to remain irreconcilable during some Late Paleocene and Eocene intervals, suggesting the breakdown of one or more of the assumptions underlying the paleothermometers, such as $\delta^{18}O_{sw}$ reconstructions and/or $^{18}\alpha$ relationships. Solving these issues will have direct implications on the constraints we can place on parameters such as climate sensitivity and polar amplification using the paleoclimate record, and more generally on our understanding of past an future climates.

Acknowledgements

Original motivation for this study grew out of MD's visit to Utrecht at the invitation of M. Ziegler and I. J. Kocken. This work benefitted in many ways from the stimulating discussions we had with M. Peral, J.-C. Duplessy, C. Waelbroeck, E. Michel, and members of the Paléoceans group at LSCE. We are grateful to N. Meinicke and N. Meckler, who graciously shared unpublished I-CDES-reprocessed calibration data. This report was greatly improved by the detailed and thoughtful comments of three reviewers, including N. Meckler's whose candid feedback was remarkably fair and constructive regardless of our differences of interpretation on some issues. We also benefitted greatly from M. Huber's editorial handling, whose suggestions substantially improved the final contents of this work.

Open Research

The complete data set and code base for this study are available at Zenodo under a Modified BSD License (*Daëron & Gray*, 2023). The preferred way to comment on the code or to suggest improvements is to raise an issue at https://github.com/mdaeron/isoForam. All data considered here are, as indicated in the text, from the original studies of *Peral et al.* (2018, 2022), *Piasecki et al.* (2019), *Meinicke et al.* (2020, 2021), *Anderson et al.* (2021), *Fiebig et al.* (2021) (clumped-isotope calibration data); *Grossman & Ku* (1986), *Spero & Lea* (1993, 1996), *Bemis et al.* (1998), *Keigwin* (1998), *Mulitza et al.* (2003), *Lončarić et al.* (2006), *McCorkle et al.* (2008), *Barras et al.* (2010), *Marchitto et al.* (2014) ($^{18}\alpha$ observations); *Rebotim et al.* (2017), *Meilland et al.* (2019), *Greco et al.* (2019) (habitat depths from stratified plankton tows); *Breitkreuz et al.* (2018) (gridded $\delta^{18}O_{sw}$ database); https://www.ncei.noaa.gov/products/world-ocean-atlas (World Ocean Atlas); *Lauvset et al.* (2016) (GLODAPv2 database); *Malevich et al.* (2019) (global compilation of planktic foraminifera from core-tops); *Meckler et al.* (2022), *Cramer et al.* (2011) (Cenozoic reconstructions of deep ocean temperature and $\delta^{18}O_{sw}$); *Westerhold et al.* (2020) (stacked benthic foraminifer $\delta^{18}O_c$ record over the Cenozoic); https://github.com/mdaeron/D47calib (OGLS23 calibration, *Daëron*, 2023).

References

Anderson, N. T., Kelson, J. R., Kele, S., Daëron, M., Bonifacie, M., Horita, J., Mackey, T. J., John, C. M., Kluge, T., Petschnig, P., Jost, A. B., Huntington, K. W., Bernasconi, S .M. & Bergmann, K. D. (2021). A Unified Clumped Isotope Thermometer Calibration (0.5–1,100 °C) Using Carbonate-Based Standardization. *Geophysical Research Letters* 48:(7). doi: 10.1029/2020gl092069.

Bajnai, D., Guo, W., Spötl, C., Coplen, T. B., Methner, K., Löffler, N., Krsnik, E., Gischler, E., Hansen, M., Henkel, D., Price, G. D., Raddatz, J., Scholz, D. & Fiebig, J. (2020). Dual clumped isotope thermometry resolves kinetic biases in carbonate formation temperatures. *Nature Communications* 11:(1). doi: 10.1038/s41467-020-17501-0.

Barras, C., Duplessy, J.-C., Geslin, E., Michel, E. & Jorissen, F. J. (2010). Calibration of $\delta^{18}O$ of cultured benthic foraminiferal calcite as a function of temperature. *Biogeosciences* 7:(4), pp. 1349–1356. doi: 10.5194/bg-7-1349-2010.

Beck, W. C., Grossman, E. L. & Morse, J. W. (2005). Experimental studies of oxygen isotope fractionation in the carbonic acid system at 15 °, 25 °, and 40 °C. *Geochimica et Cosmochimica Acta* 69:(14), pp. 3493–3503. doi: 10.1016/j.gca.2005.02.003.

Bemis, B. E., Spero, H. J., Bijma, J. & Lea, D. W. (1998). Reevaluation of the oxygen isotopic composition of planktonic foraminifera: Experimental results and revised paleotemperature equations. *Paleoceanography* 13:(2), pp. 150–160. doi: doi.org/10.1029/98PA00070.

Bernard, S., Daval, D., Ackerer, P., Pont, S. & Meibom, A. (2017). Burial-induced oxygen-isotope re-equilibration of fossil foraminifera explains ocean paleotemperature paradoxes. *Nature Communications* 8:(1). doi: 10.1038/s41467-017-01225-9.

Bernasconi, S. M., Daëron, M., Bergmann, K. D., Bonifacie, M., Meckler, A. N., Affek, H. P., Anderson, N., Bajnai, D., Barkan, E., Beverly, E., Blamart, D., Burgener, L., Calmels, D., Chaduteau, C., Clog, M., Davidheiser-Kroll, B., Davies, A., Dux, F., Eiler, J. M., Elliot, B., Fetrow, A. C., Fiebig, J., Goldberg, S., Hermoso, M., Huntington, K. W., Hyland, E., Ingalls, M., Jaggi, M., John, C. M., Jost, A. B., Katz, S., Kelson, J., Kluge, T., Kocken, I. J., Laskar, A., Leutert, T. J., Liang, D., Lucarelli, J., Mackey, T. J., Mangenot, X., Meinicke, N., Modestou, S. E., Müller, I. A., Murray, S., Neary, A., Packard, N., Passey, B. H., Pelletier, E., Petersen, S., Piasecki, A., Schauer, A., Snell, K. E., Swart, P. K., Tripati, A., Upadhyay, D., Vennemann, T., Winkelstern, I., Yarian, D., Yoshida, N., Zhang, N. & Ziegler, M. (2021). InterCarb: A community effort to improve inter-laboratory standardization of the carbonate clumped isotope thermometer using carbonate standards. *Geochemistry, Geophysics, Geosystems* 22:(5). doi: 10.1029/2020GC009588.

Bernasconi, S. M., Müller, I. A., Bergmann, K. D., Breitenbach, S. F. M., Fernandez, A., Hodell, D. A., Meckler, A. N., Millan, I. & Ziegler, M. (2018). Reducing uncertainties in carbonate clumped isotope analysis through consistent carbonate-based standardization. *Geochemistry, Geophysics, Geosystems* 19. doi: 10.1029/2017GC007385.

Bigeleisen, J. & Goeppert Mayer, M.. (1947). Calculation of Equilibrium Constants for Isotopic Exchange Reactions. *The Journal of Chemical Physics* 15:(5), pp. 261–267. doi: 10.1063/1.1746492.

Breitkreuz, C., Paul, A., Kurahashi-Nakamura, T., Losch, M. & Schulz, M. (2018). A dynamical reconstruction of the global monthly mean oxygen isotopic composition of seawater. *Journal of Geophysical Research: Oceans* 123:(10), pp. 7206–7219. doi: 10.1029/2018jc014300.

Caron, D. A., Roger Anderson, O., Lindsey, J. L., Faber, W. W. & Lin Lim, E.E. (1990). Effects of gametogenesis on test structure and dissolution of some spinose planktonic foraminifera and implications for test preservation. *Marine Micropaleontology* 16:(1-2), pp. 93–116. doi: 10.1016/0377-8398(90)90031-g.

Cisneros-Lazaro, D., Adams, A., Guo, J., Bernard, S., Baumgartner, L. P., Daval, D., Baronnet, A., Grauby, O., Vennemann, T., Stolarski, J., Escrig, S. & Meibom, A. (2022). Fast and pervasive diagenetic isotope exchange in foraminifera tests is species-dependent. *Nature Communications* 13:(1). doi: 10.1038/s41467-021-27782-8.

Cleveland, W. S. (1979). Robust Locally Weighted Regression and Smoothing Scatterplots. *Journal of the American Statistical Association* 74:(368), pp. 829–836. doi: 10.1080/01621459.1979.10481038.

Cleveland, W. S. & Devlin, S. J. (1988). Locally Weighted Regression: An Approach to Regression Analysis by Local Fitting. *Journal of the American Statistical Association* 83:(403), pp. 596–610. doi: 10.1080/01621459.1988.10478639.

Coplen, T. B. (2007). Calibration of the calcite-water oxygen-isotope geothermometer at Devils Hole, Nevada, a natural laboratory. *Geochimica et Cosmochimica Acta* 71:(16), pp. 3948–3957. doi: 10.1016/j.gca.2007.05.028.

Craig, H. (1965). The measurement of oxygen isotope paleotemperatures. *Stable Isotopes in Oceanographic Studies and Paleotemperatures*. Edited by E. Tongiorgi. Consiglio Nazionale delle Ricerche, Laboratorio de Geologia Nucleare, Pisa.

Cramer, B. S., Miller, K. G., Barrett, P. J. & Wright, J. D. (2011). Late Cretaceous–Neogene trends in deep ocean temperature and continental ice volume: Reconciling records of benthic foraminiferal geochemistry ($\delta^{18}O$ and Mg/Ca) with sea level history. *Journal of Geophysical Research* 116:(C12). doi: 10.1029/2011jc007255.

Cramwinckel, M. J., Huber, M., Kocken, I. J., Agnini, C., Bijl, P. K., Bohaty, S. M., Frieling, J., Goldner, A., Hilgen, F. J., Kip, E. L., Peterse, F., Ploeg, R. van der, Röhl, U., Schouten, S. & Sluijs, A. (2018). Synchronous tropical and polar temperature evolution in the Eocene. *Nature* 559:(7714), pp. 382–386. doi: 10.1038/s41586-018-0272-2.

Daëron, M. (2021). Full propagation of analytical uncertainties in Δ_{47} measurements. *Geochemistry, Geophysics, Geosystems* 22:(5). doi: 10.1029/2020gc009592.

Daëron, M. (2023). *mdaeron/D47calib: D47calib (v1.2). [Software]. Zenodo.* doi: 10.5281/zenodo.8360217.

Daëron, M., Drysdale, R. N., Peral, M., Huyghe, D., Blamart, D., Coplen, T. B., Lartaud, F. & Zanchetta, G. (2019). Most Earth-surface calcites precipitate out of isotopic equilibrium. *Nature Communications* 10:(1). doi: 10.1038/s41467-019-08336-5.

Daëron, M. & Gray, W. R. (2023). *mdaeron/isoForam: isoForam (v1.0). [Software]. Zenodo.* doi: 10.5281/zenodo.8367191.

Daëron, M. & Vermeesch, P. (2023). Omnivariant Generalized Least Squares Regression: Theory, Geochronological Applications, and Making the Case for Reconciled Δ_{47} calibrations. Preprint (in review, *Chemical Geology*). URL: https://hal.science/hal-04211269.

Davies, A.J., Guo, W., Bernecker, M., Tagliavento, M., Raddatz, J., Gischler, E., Flögel, S. & Fiebig, J. (2022). Dual clumped isotope thermometry of coral carbonate. *Geochimica et Cosmochimica Acta* 338, pp. 66–78. doi: 10.1016/j.gca.2022.10.015.

Dennis, K. J., Affek, H. P., Passey, B. H., Schrag, D. P. & Eiler, J. M. (2011). Defining an absolute reference frame for 'clumped' isotope studies of CO_2. *Geochimica et Cosmochimica Acta* 75, pp. 7117–7131. doi: 10.1016/j.gca.2011.09.025.

Devriendt, L. S., Watkins, J. M. & McGregor, H. V. (2017). Oxygen isotope fractionation in the $CaCO_3$-DIC-H_2O system. *Geochimica et Cosmochimica Acta* 214, pp. 115–142. doi: 10.1016/j.gca.2017.06.022.

Duplessy, J.-C., Blanc, P.-L. & Bé, A. W. H. (1981). Oxygen-18 Enrichment of Planktonic Foraminifera Due to Gametogenic Calcification Below the Euphotic Zone. *Science* 213:(4513), pp. 1247–1250. doi: 10.1126/science.213.4513.1247.

Duplessy, J.-C., Lalou, C. & Vinot, A. C. (1970). Differential Isotopic Fractionation in Benthic Foraminifera and Paleotemperatures Reassessed. *Science* 168:(3928), pp. 250–251. doi: 10.1126/science.168.3928.250.

Eiler, J. M. (2011). Paleoclimate reconstruction using carbonate clumped isotope thermometry. *Quaternary Science Reviews* 30, pp. 3575–3588. doi: 10.1016/j.quascirev.2011.09.001.

Emiliani, C. (1954a). Depth habitats of some species of pelagic Foraminifera as indicated by oxygen isotope ratios. *American Journal of Science* 252:(3), pp. 149–158. doi: 10.2475/ajs.252.3.149.

Emiliani, C. (1954b). Temperatures of Pacific Bottom Waters and Polar Superficial Waters during the Tertiary. *Science* 119:(3103), pp. 853–855. doi: 10.1126/science.119.3103.853.

Epstein, S., Buchsbaum, R., Lowenstam, H. A. & Urey, H. C. (1953). Revised carbonate-water isotopic temperature scale. *Geological Society of America Bulletin* 64:(11), pp. 1315. doi: 10.1130/0016-7606(1953)64[1315:rcits]2.0.co;2.

Erez, J. & Luz, B. (1983). Experimental paleotemperature equation for planktonic foraminifera. *Geochimica et Cosmochimica Acta* 47:(6), pp. 1025–1031. doi: 10.1016/0016-7037(83)90232-6.

Fiebig, J., Daëron, M., Bernecker, M., Guo, W., Schneider, G., Boch, R., Bernasconi, S. M., Jautzy, J. & Dietzel, M. (2021). Calibration of the dual clumped isotope thermometer for carbonates. *Geochimica et Cosmochimica Acta* 312, pp. 235–256. doi: 10.1016/j.gca.2021.07.012.

Gaskell, D. E., Huber, M., O'Brien, C. L., Inglis, G. N., Acosta, R. P., Poulsen, C. J. & Hull, P. M. (2022). The latitudinal temperature gradient and its climate dependence as inferred from foraminiferal $\delta^{18}O$ over the past 95 million years. *Proceedings of the National Academy of Sciences* 119:(11). doi: 10.1073/pnas.2111332119.

Grauel, A.-L., Schmid, T. W., Hu, B., Bergami, C., Capotondi, L., Zhou, L. & Bernasconi, S. M. (2013). Calibration and application of the 'clumped isotope' thermometer to foraminifera for high-resolution climate reconstructions. *Geochimica et Cosmochimica Acta* 108, pp. 125–140. doi: 10.1016/j.gca.2012.12.049.

Greco, M., Jonkers, L., Kretschmer, K., Bijma, J. & Kucera, M. (2019). Depth habitat of the planktonic foraminifera *Neogloboquadrina pachyderma* in the northern high latitudes explained by sea-ice and chlorophyll concentrations. *Biogeosciences* 16:(17), pp. 3425–3437. doi: 10.5194/bg-16-3425-2019.

Grossman, E. L. & Ku, T.-L. (1986). Oxygen and carbon isotope fractionation in biogenic aragonite: Temperature effects. *Chemical Geology* 59, pp. 59–74. doi: 10.1016/0168-9622(86)90057-6.

Hamilton, C. P., Spero, H. J., Bijma, J. & Lea, D. W. (2008). Geochemical investigation of gametogenic calcite addition in the planktonic foraminifera Orbulina universa. *Marine Micropaleontology* 68:(3-4), pp. 256–267. doi: 10.1016/j.marmicro.2008.04.003.

Hansen, J., Sato, M., Russell, G. & Kharecha, P. (2013). Climate sensitivity, sea level and atmospheric carbon dioxide. *Philosophical Transactions of the Royal Society A: Mathematical, Physical and Engineering Sciences* 371:(2001), pp. 20120294. doi: 10.1098/rsta.2012.0294.

Huyghe, D., Daëron, M., Rafelis, M. de, Blamart, D., Sébilo, M., Paulet, Y.-M. & Lartaud, F. (2022). Clumped isotopes in modern marine bivalves. *Geochimica et Cosmochimica Acta* 316, pp. 41–58. doi: 10.1016/j.gca.2021.09.019.

Keigwin, L. D. (1998). Glacial-age hydrography of the far northwest Pacific Ocean. *Paleoceanography* 13:(4), pp. 323–339. doi: 10.1029/98pa00874.

Kim, S.-T. & O'Neil, J. R. (1997). Equilibrium and nonequilibrium oxygen isotope effects in synthetic carbonates. *Geochimica et Cosmochimica Acta* 61:(16), pp. 3461–3475. doi: 10.1016/s0016-7037(97)00169-5.

Kohn, R., Schimek, M. G. & Smith, M. (2000). Spline and Kernel Regression for Dependent Data. *Wiley Series in Probability and Statistics*, pp. 135–158. doi: 10.1002/9781118150658.ch6.

Lauvset, S. K., Key, R. M., Olsen, A., Heuven, S. van, Velo, A., Lin, X., Schirnick, C., Kozyr, A., Tanhua, T., Hoppema, M., Jutterström, S., Steinfeldt, R., Jeansson, E., Ishii, M., Perez, F. F., Suzuki, T. & Watelet, S. (2016). A new global interior ocean mapped climatology: the 1° × 1° GLODAP version 2. *Earth System Science Data* 8:(2), pp. 325–340. doi: 10.5194/essd-8-325-2016.

LeGrande, A. N. & Schmidt, G. A. (2006). Global gridded data set of the oxygen isotopic composition in seawater. *Geophysical Research Letters* 33:(12). doi: 10.1029/2006gl026011.

Letulle, T., Gaspard, D., Daëron, M., Arnaud-Godet, F., Vinçon-Laugier, A., Suan, G. & Lécuyer, C. (2022). Multi-proxy assessment of brachiopod shell calcite as a potential archive of seawater temperature and oxygen isotope composition. *Biogeosciences* 20:(7), pp. 1381–1403. doi: 10.5194/bg-20-1381-2023.

Locarnini, R. A., Mishonov, A. V., Baranova, O. K., Boyer, T. P., Zweng, M. M., Garcia, H. E., Reagan, J. R., Seidov, D., Weathers, K. W., Paver, C. R. & Smolyar, I. V. (2018). *World Ocean Atlas 2018, Volume 1: Temperature*. Edited by A. Mishonov. NOAA Atlas NESDIS.

Lombard, F., Labeyrie, L., Michel, E., Spero, H. J. & Lea, D. W. (2009). Modelling the temperature dependent growth rates of planktic foraminifera. *Marine Micropaleontology* 70:(1–2), pp. 1–7. doi: 10.1016/j.marmicro.2008.09.004.

Lončarić, N., Peeters, F. J. C., Kroon, D. & Brummer, G.-J. A. (2006). Oxygen isotope ecology of recent planktic foraminifera at the central Walvis Ridge (SE Atlantic). *Paleoceanography* 21:(3). doi: 10.1029/2005pa001207.

Malevich, S. B., Vetter, L. & Tierney, J. E. (2019). Global Core Top Calibration of $\delta^{18}O$ in Planktic Foraminifera to Sea Surface Temperature. *Paleoceanography and Paleoclimatology* 34:(8), pp. 1292–1315. doi: 10.1029/2019pa003576.

Marchitto, T.M., Curry, W.B., Lynch-Stieglitz, J., Bryan, S.P., Cobb, K.M. & Lund, D.C. (2014). Improved oxygen isotope temperature calibrations for cosmopolitan benthic foraminifera. *Geochimica et Cosmochimica Acta* 130, pp. 1–11. doi: 10.1016/j.gca.2013.12.034.

McCave, I.N., Carter, L. & Hall, I.R. (2008). Glacial-interglacial changes in water mass structure and flow in the SW Pacific Ocean. *Quaternary Science Reviews* 27:(19–20), pp. 1886–1908. doi: 10.1016/j.quascirev.2008.07.010.

McCorkle, D. C., Bernhard, J. M., Hintz, C. J., Blanks, J. K., Chandler, G. T. & Shaw, T. J. (2008). The carbon and oxygen stable isotopic composition of cultured benthic foraminifera. *Geological Society, London, Special Publications* 303:(1), pp. 135–154. doi: 10.1144/sp303.10.

Meckler, A. N., Sexton, P. F., Piasecki, A. M., Leutert, T. J., Marquardt, J., Ziegler, M., Agterhuis, T., Lourens, L. J., Rae, J. W. B., Barnet, J., Tripati, A. & Bernasconi, S. M. (2022). Cenozoic evolution of deep ocean temperature from clumped isotope thermometry. *Science* 377:(6601), pp. 86–90. doi: 10.1126/science.abk0604.

Meilland, J., Siccha, M., Weinkauf, M. F. G., Jonkers, L., Morard, R., Baranowski, U., Baumeister, A., Bertlich, J., Brummer, G.-J., Debray, P., Fritz-Endres, T., Groeneveld, J., Magerl, L., Munz, P., Rillo, M. C, Schmidt, C., Takagi, H., Theara, G. & Kucera, M. (2019). Highly replicated sampling reveals no diurnal vertical migration but stable species-specific vertical habitats in planktonic foraminifera. *Journal of Plankton Research* 41:(2), pp. 127–141. doi: 10.1093/plankt/fbz002.

Meinicke, N., Ho, S.L., Hannisdal, B., Nürnberg, D., Tripati, A., Schiebel, R. & Meckler, A.N. (2020). A robust calibration of the clumped isotopes to temperature relationship for foraminifers. *Geochimica et Cosmochimica Acta* 270, pp. 160–183. doi: 10.1016/j.gca.2019.11.022.

Meinicke, N., Reimi, M. A., Ravelo, A. C. & Meckler, A. N. (2021). Coupled Mg/Ca and Clumped Isotope Measurements Indicate Lack of Substantial Mixed Layer Cooling in the Western Pacific Warm Pool During the Last ∼5 Million Years. *Paleoceanography and Paleoclimatology* 36:(8). doi: 10.1029/2020pa004115.

Mulitza, S., Boltovskoy, D., Donner, B., Meggers, H., Paul, A. & Wefer, G. (2003). Temperature:$\delta^{18}O$ relationships of planktonic foraminifera collected from surface waters. *Palaeogeography, Palaeoclimatology, Palaeoecology* 202:(1–2), pp. 143–152. doi: 10.1016/s0031-0182(03)00633-3.

O'Neil, J. R., Clayton, R. N. & Mayeda, T. K. (1969). Oxygen isotope fractionation in divalent metal carbonates. *The Journal of Chemical Physics* 51:(12), pp. 5547–5558. doi: 10.1063/1.1671982.

Peral, M., Bassinot, F., Daëron, M., Blamart, D., Bonnin, J., Jorissen, F., Kissel, C., Michel, E., Waelbroeck, C., Rebaubier, H. & Gray, W. R. (2022). On the combination of the planktonic foraminiferal Mg/Ca, clumped (Δ_{47}) and conventional ($\delta^{18}O$) stable isotope paleothermometers in palaeoceanographic studies. *Geochimica et Cosmochimica Acta* 339, pp. 22–34. doi: 10.1016/j.gca.2022.10.030.

Peral, M., Daëron, M., Blamart, D., Bassinot, F., Dewilde, F., Smialkowski, N., Isguder, G., Bonnin, J., Jorissen, F., Kissel, C., Michel, E., Vázquez Riveiros, N. & Waelbroeck, C. (2018). Updated calibration of the clumped isotope thermometer in planktonic and benthic foraminifera. *Geochimica et Cosmochimica Acta* 239, pp. 1–16. doi: 10.1016/j.gca.2018.07.016.

Piasecki, A., Bernasconi, S. M., Grauel, A.-L., Hannisdal, B., Ho, S. L., Leutert, T. J., Marchitto, T. M., Meinicke, N., Tisserand, A. & Meckler, N. (2019). Application of Clumped Isotope Thermometry to Benthic Foraminifera. *Geochemistry, Geophysics, Geosystems* 20:(4), pp. 2082–2090. doi: 10.1029/2018gc007961.

Rebotim, A., Voelker, A. H. L., Jonkers, L., Waniek, J. J., Meggers, H., Schiebel, R., Fraile, I., Schulz, M. & Kucera, M. (2017). Factors controlling the depth habitat of planktonic foraminifera in the subtropical eastern North Atlantic. *Biogeosciences* 14:(4), pp. 827–859. doi: 10.5194/bg-14-827-2017.

Roche, D. M., Waelbroeck, C., Metcalfe, B. & Caley, T. (2018). FAME (v1.0): a simple module to simulate the effect of planktonic foraminifer species-specific habitat on their oxygen isotopic content. *Geoscientific Model Development* 11:(9), pp. 3587–3603. doi: 10.5194/gmd-11-3587-2018.

Roy, P. T., Owen, A. B., Balandat, M. & Haberland, M. (2023). Quasi-Monte Carlo Methods in Python. *Journal of Open Source Software* 8:(84), pp. 5309. doi: 10.21105/joss.05309.

Saenger, C., Affek, H. P., Felis, T., Thiagarajan, N., Lough, J. M. & Holcomb, M. (2012). Carbonate clumped isotope variability in shallow water corals: Temperature dependence and growth-related vital effects. *Geochimica et Cosmochimica Acta* 99, pp. 224–242. doi: 10.1016/j.gca.2012.09.035.

Schiebel, R., Smart, S. M., Jentzen, A., Jonkers, L., Morard, R., Meilland, J., Michel, E., Coxall, H. K., Hull, P. M., Garidel-Thoron, T. de, Aze, T., Quillévéré, F., Ren, H., Sigman, D. M., Vonhof, H. B., Martínez-García, A., Kučera, M., Bijma, J., Spero, H. J. & Haug, G. H. (2018). Advances in planktonic foraminifer research: New perspectives for paleoceanography. *Revue de Micropaléontologie* 61:(3–4), pp. 113–138. doi: 10.1016/j.revmic.2018.10.001.

Schmiedl, G. & Mackensen, A. (2006). Multispecies stable isotopes of benthic foraminifers reveal past changes of organic matter decomposition and deepwater oxygenation in the Arabian Sea. *Paleoceanography* 21:(4). doi: 10.1029/2006pa001284.

Shackleton, N. J. (1967). Oxygen isotope analyses and Pleistocene temperatures re-assessed. *Nature* 215, pp. 15–17. doi: 10.1038/215015a0.

Shackleton, N. J. (1974). Attainment of isotopic equilibrium between ocean water and the benthonic foraminifera genus Uvigerina: isotopic changes in the ocean during the last glacial. *Colloques Internationaux du CNRS* 219, pp. 203–210.

Shackleton, N. J., Wiseman, J. D. H. & Buckley, H. A. (1973). Non-equilibrium Isotopic Fractionation between Seawater and Planktonic Foraminiferal Tests. *Nature* 242:(5394), pp. 177–179. doi: 10.1038/242177a0.

Spero, H. J. (1992). Do planktic foraminifera accurately record shifts in the carbon isotopic composition of seawater ΣCO_2? *Marine Micropaleontology* 19:(4), pp. 275–285. doi: 10.1016/0377-8398(92)90033-g.

Spero, H. J., Bijma, J., Lea, D. W. & Bemis, B. E. (1997). Effect of seawater carbonate concentration on foraminiferal carbon and oxygen isotopes. *Nature* 390:(6659), pp. 497–500. doi: 10.1038/37333.

Spero, H. J. & Lea, D. W. (1993). Intraspecific stable isotope variability in the planktic foraminifera *Globigerinoides sacculifer*: Results from laboratory experiments. *Marine Micropaleontology* 22:(3), pp. 221–234. doi: 10.1016/0377-8398(93)90045-y.

Spero, H. J. & Lea, D. W. (1996). Experimental determination of stable isotope variability in *Globigerina bulloides*: implications for paleoceanographic reconstructions. *Marine Micropaleontology* 28:(3–4), pp. 231–246. doi: 10.1016/0377-8398(96)00003-5.

Tarutani, T., Clayton, R. N & Mayeda, T. K (1969). The effect of polymorphism and magnesium substitution on oxygen isotope fractionation between calcium carbonate and water. *Geochimica et Cosmochimica Acta* 33:(8), pp. 987–996. doi: 10.1016/0016-7037(69)90108-2.

Tierney, J. E., Poulsen, C. J., Montañez, I. P., Bhattacharya, T., Feng, R., Ford, H. L., Hönisch, B., Inglis, G. N., Petersen, S. V., Sagoo, N., Tabor, C. R., Thirumalai, K., Zhu, J., Burls, N. J., Foster, G. L., Goddéris, Y., Huber, B. T., Ivany, L. C., Kirtland Turner, S., Lunt, D. J., McElwain, J. C., Mills, B. J. W., Otto-Bliesner, B. L., Ridgwell, A. & Zhang, Y. G. (2020). Past climates inform our future. *Science* 370:(6517). doi: 10.1126/science.aay3701.

Tripati, A. K., Eagle, R. A., Thiagarajan, N., Gagnon, A. C., Bauch, H., Halloran, P. R. & Eiler, J. M. (2010). ^{13}C–^{18}O isotope signatures and 'clumped isotope' thermometry in foraminifera and coccoliths. *Geochimica et Cosmochimica Acta* 74:(20), pp. 5697–5717. doi: 10.1016/j.gca.2010.07.006.

Urey, H. C. (1947). The thermodynamic properties of isotopic substances. *Journal of the Chemical Society*, pp. 562–581. doi: 10.1039/JR9470000562.

Watkins, J. M. & Hunt, J. D. (2015). A process-based model for non-equilibrium clumped isotope effects in carbonates. *Earth and Planetary Science Letters* 432, pp. 152–165. doi: 10.1016/j.epsl.2015.09.042.

Watkins, J. M., Hunt, J. D., Ryerson, F. J. & DePaolo, D. J. (2014). The influence of temperature, pH, and growth rate on the $\delta^{18}O$ composition of inorganically precipitated calcite. *Earth and Planetary Science Letters* 404, pp. 332–343. doi: 10.1016/j.epsl.2014.07.036.

Weldeab, S., Lea, D. W., Schneider, R. R. & Andersen, N. (2007). 155,000 Years of West African Monsoon and Ocean Thermal Evolution. *Science* 316:(5829), pp. 1303–1307. doi: 10.1126/science.1140461.

Westerhold, T., Marwan, N., Drury, A. J., Liebrand, D., Agnini, C., Anagnostou, E., Barnet, J. S. K., Bohaty, S. M., De Vleeschouwer, D., Florindo, F., Frederichs, T., Hodell, D. A., Holbourn, A. E., Kroon, D., Lauretano, V., Littler, K., Lourens, L. J., Lyle, M., Pälike, H., Röhl, U., Tian, J., Wilkens, R. H., Wilson, P. A. & Zachos, J. C. (2020). An astronomically dated record of Earth's climate and its predictability over the last 66 million years. *Science* 369:(6509), pp. 1383–1387. doi: 10.1126/science.aba6853.

York, D., Evensen, N. M., López Martínez, M. & De Basabe Delgado, J. (2004). Unified equations for the slope, intercept, and standard errors of the best straight line. *American Journal of Physics* 72:(3), pp. 367–375. doi: 10.1119/1.1632486.

Zeebe, R. E., Bijma, J., Hönisch, B., Sanyal, A., Spero, H. J. & Wolf-Gladrow, D. A. (2008). Vital effects and beyond: a modelling perspective on developing palaeoceanographical proxy relationships in foraminifera. *Geological Society, London, Special Publications* 303:(1), pp. 45–58. doi: 10.1144/sp303.4.

Core	Latitude	Longitude	Depth (m)	Bottom Temperature (°C)	Bottom Salinity (g/kg)	Bottom Saturation ($\Omega_{calcite}$)	Bottom $\delta^{18}O_{sw}$ (‰ VSMOW)	Original study
MOCOSED	73.04	−11.93	1839	−0.8 ± 0.5	34.91	1.6	0.29	*Peral et al.* (2018)
MD04-2720	−49.13	71.36	750	2.3 ± 0.1	34.62	1.5	−0.15	—
MD12-3401	−44.69	80.40	3445	1.2 ± 0.5	34.74	1.0	−0.11	—
MD95-2014	60.59	−22.08	2397	2.8 ± 0.5	34.97	1.5	0.18	—
MD08-3182	52.71	−35.94	1355	3.4 ± 0.1	34.90	1.9	0.21	—
MD03-2680	61.06	−24.55	1812	3.0 ± 0.5	34.96	1.7	0.22	—
2FPA1	43.67	−2.00	664	10.6 ± 0.1	35.61	2.8	0.74	—
SU90-03	40.05	−30.00	2475	3.3 ± 0.5	34.93	1.5	0.18	—
MD08-3179	37.86	−30.30	2036	3.8 ± 0.5	34.99	1.7	0.20	—
MD12-3426	19.73	114.61	3630	2.4 ± 0.5	34.68	0.8	−0.13	—
MD00-2360	−20.08	112.67	980	5.1 ± 0.5	34.63	1.4	−0.05	—
MD02-2577	28.84	−86.67	4076	4.3 ± 0.5	34.89	1.1	0.11	—
13MC-G	24.37	−83.24	348	10.6 ± 0.1	35.69	3.4	0.54	*Piasecki et al.* (2019)
19MC-G	24.42	−83.21	173	15.4 ± 0.7	36.47	4.8	0.93	—
50MC-G	24.41	−83.22	198	14.3 ± 0.5	36.45	4.5	0.86	—
53MC-G	24.38	−83.23	302	11.6 ± 0.3	36.00	3.9	0.61	—
89MC-G	24.56	−79.24	353	15.2 ± 0.5	35.96	3.7	0.54	—
94MC-G	24.57	−79.23	259	18.1 ± 0.5	36.37	4.1	0.71	—
GS06-144-19	63.83	5.27	830	−0.5 ± 0.1	34.90	2.0	0.29	—
GS07-150-17-2	−4.47	−37.21	1000	4.2 ± 0.1	34.57	1.5	0.13	—
GS07-150-22-1	−4.33	−37.16	598	6.1 ± 0.1	34.47	1.8	0.05	—
MP43-BC	39.72	16.97	246	14.3 ± 0.1	38.98	4.5	1.57	—
MP46-MC	39.54	17.25	582	13.9 ± 0.1	38.81	4.5	1.61	—
SO213-54-4	−43.72	−120.67	3840	1.5 ± 0.5	34.71	0.9	−0.15	—
SO213-71-2	−45.58	−157.90	689	6.9 ± 0.1	34.37	2.1	0.03	—
GS15-198-63MC	70.50	−2.80	2995	−0.8 ± 0.5	34.91	1.3	0.49	*Meinicke et al.* (2020)
GS15-198-38MC	70.10	−17.70	1610	−0.8 ± 0.5	34.91	1.6	0.27	—
GS15-198-62MC	70.00	−13.60	1423	−0.8 ± 0.1	34.91	1.7	0.26	—
GS06-144-19MC	63.80	5.20	922	−0.6 ± 0.5	34.90	1.9	0.28	—
CD107 A ML 5A	52.90	−16.90	3569	2.5 ± 0.5	34.92	1.2	0.15	—
CD94 17B	48.90	−11.80	1484	5.3 ± 0.2	35.10	1.9	0.36	—
KL88	34.80	−27.70	2060	3.6 ± 0.5	35.00	1.7	0.20	—
CD145 A150	23.30	66.70	151	20.3 ± 0.4	36.35	2.2	0.74	—
SO164-25-3	14.70	−59.70	2720	2.8 ± 0.5	34.94	1.4	0.18	—
OJP2016 MW0691 1.5BC11	−1.00	157.80	2016	2.2 ± 0.5	34.64	1.1	−0.09	—
WIND 33B	−11.20	58.80	2871	1.8 ± 0.5	34.73	1.1	−0.05	—
SO225-53-1	−13.50	−162.10	3154	1.7 ± 0.5	34.68	1.0	−0.13	—
SO213-84-2	−45.10	174.60	992	3.7 ± 0.1	34.42	2.0	−0.11	—

Table 1 — Core-top sites considered in this study, with bottom temperatures from WOA23, $\delta^{18}O_{sw}$ (*Breitkreuz et al.*, 2018), salinity and calcite saturation (GLODAPv2: *Lauvset et al.*, 2016).

Study	Genus / Species	N	T (°C)	Foraminifera from
Grossman & Ku (1986)	*Hoeglundina elegans* (arag.)	52	3 – 20	offshore stations
	Uvigerina curticosta	8	4 – 7	
	Uvigerina flintii	4	13 – 17	
	Uvigerina peregrina	8	3 – 12	
Spero & Lea (1993)	*Orbulina universa*	6	∼ 29	culture experiments
Spero & Lea (1996)	*Globigerina bulloides*	9	∼ 16	culture experiments
Bemis et al. (1998)	*Globigerina bulloides*	17	15 – 24	culture experiments
	Orbulina universa	14	15 – 25	
Keigwin (1998)	*Cibicidoides*	21	∼ 2	Holocene core tops
	Uvigerina	27	∼ 2	
Mulitza et al. (2003)	*Globigerina bulloides*	21	2 – 26	depth-stratified plankton tows
	Globigerinoides ruber white	91	16 – 31	
	Globigerinoides sacculifer	68	16 – 31	
	Neogloboquadrina pachyderma (s.)	49	−2 – 13	
Lončarić et al. (2006)	*Globorotalia inflata*	13	14 – 19	depth-stratified plankton tows
	Globorotalia truncatulinoides (d.)	10	13 – 19	
	Globorotalia truncatulinoides (s.)	22	13 – 19	
McCorkle et al. (2008)	*Bulimina aculeata*	43	∼ 7	culture experiments
	Rosalina vilardeboana	24	∼ 7	
Barras et al. (2010)	*Bulimina marginata*	83	4 – 19	culture experiments
Marchitto et al. (2014)	*Cibicidoides pachyderma*	28	6 – 19	Holocene core tops
	Cibicidoides wuellerstorfi	27	−1 – 0	
	Hoeglundina elegans (arag.)	63	4 – 26	
	Planulina ariminensis	9	7 – 12	
	Planulina foveolata	10	11 – 18	
	Uvigerina peregrina	19	6 – 17	

Table 2 — Studies used here to constrain how the oxygen-18 fractionation ($^{18}\alpha$) between seawater and foraminiferal $CaCO_3$ varies with temperature. Results summarized in figs. 3-5.

Reference	Species	Depths (m)
Rebotim et al. (2017)	*Berggrenia pumillio*	30 – 200
	Globigerinella calida	30 – 120
	Globigerinella siphonifera	50 – 200
	Globigerinita glutinata	25 – 200
	Globorotalia crassaformis	30 – 60
	Globorotalia inflata	30 – 200
	Globorotalia truncatulinoides	40 – 250
	Globorotalia truncatulinoides (d.)	40 – 250
	Globorotalia truncatulinoides (s.)	40 – 250
	Globoturborotalita rubescens	30 – 350
	Tenuitella fleisheri	35 – 150
	Tenuitella iota	40 – 400
	Tenuitella parkerae	50 – 300
	Trilobatus trilobus	15 – 200
	Turborotalita humilis	30 – 200
Greco et al. (2019)	*Neogloboquadrina pachyderma*	25 – 280
Meilland et al. (2019)	*Beella digitata*	20 – 250
	Berggrenia pumilio	30 – 60
	Candeina nitida	0 – 80
	Dentigloborotalia anfracta	0 – 100
	Globigerina calida	0 – 180
	Globigerina crassaformis	80 – 240
	Globigerina glutinata	0 – 100
	Globigerina radians	0 – 120
	Globigerina rubescens	0 – 100
	Globigerina siphonifera	0 – 160
	Globigerinoides conglobatus	0 – 50
	Globigerinoides elongatus	0 – 110
	Globorotalia menardii	0 – 120
	Globorotalia tumida	0 – 110
	Globorotalia ungulata	30 – 70
	Orbulina universa	10 – 130
	Tenuitellita fleisheri	0 – 230
	Tenuitellita iota	0 – 40
	Tenuitellita parkerae	0 – 90
	Truncatulina humilis	0 – 110
Meilland et al. (2019)	*Globigerina bulloides*	0 – 300
Rebotim et al. (2017)	*Globigerina falconensis*	30 – 200
	Globigerinoides ruber pink	0 – 100
	Globigerinoides ruber white	0 – 120
	Globigerinoides tenellus	0 – 160
	Globorotalia hirsuta	20 – 400
	Globorotalia scitula	10 – 400
	Hastigerina pelagica	20 – 300
	Neogloboquadrina dutertrei	0 – 130
	Neogloboquadrina incompta	0 – 200
	Pulleniatina obliquiloculata	0 – 100
	Trilobatus sacculifer	0 – 200
	Turborotalita clarkei	0 – 300
	Turborotalita quinqueloba	0 – 400

Table 3 — Best estimates of habitat depth ranges for planktic species. Depth intervals from *Rebotim et al.* (2017) are interquartile ranges from their fig. 7. Depth intervals from *Meilland et al.* (2019) are 95 % coverage intervals based on their supplemental table S2. For species present more than one study, the range reported here is the union of both intervals. Depth interval for *N. pachyderma* is quoted verbatim from *Greco et al.* (2019).

Category	A / 1000	B (± SE)	SD	References
Species:				
Globigerina bulloides	18.03	−32.47 ± 0.031	0.21	*Bemis et al.* (1998) fig 1c *Mulitza et al.* (2003) *Spero & Lea* (1996)
Globigerinoides ruber white	18.03	−32.75 ± 0.022	0.21	*Mulitza et al.* (2003)
Globorotalia inflata	18.03	−32.05 ± 0.063	0.23	*Lončarić et al.* (2006)
Globorotalia truncatulinoides (d.)	18.03	−32.20 ± 0.102	0.32	*Lončarić et al.* (2006)
Globorotalia truncatulinoides (s.)	18.03	−32.10 ± 0.049	0.23	*Lončarić et al.* (2006)
Neogloboquadrina pachyderma	18.03	−32.32 ± 0.045	0.31	*Mulitza et al.* (2003)
Orbulina universa	18.03	−31.95 ± 0.041	0.18	*Bemis et al.* (1998) fig 1a *Spero & Lea* (1993)
Trilobatus sacculifer	18.03	−32.67 ± 0.027	0.22	*Mulitza et al.* (2003)
Bulimina aculeata	18.03	−31.87 ± 0.020	0.13	*McCorkle et al.* (2008)
Bulimina marginata	18.03	−31.99 ± 0.014	0.12	*Barras et al.* (2010)
Cibicidoides pachyderma	18.03	−32.22 ± 0.025	0.13	*Marchitto et al.* (2014)
Cibicidoides wuellerstorfi	18.03	−32.24 ± 0.018	0.09	*Marchitto et al.* (2014)
Hoeglundina elegans	18.03	−31.06 ± 0.026	0.27	*Grossman & Ku* (1986) *Marchitto et al.* (2014)
Planulina ariminensis	18.03	−32.26 ± 0.044	0.13	*Marchitto et al.* (2014)
Planulina foveolata	18.03	−32.32 ± 0.056	0.18	*Marchitto et al.* (2014)
Rosalina vilardeboana	18.03	−32.18 ± 0.025	0.12	*McCorkle et al.* (2008)
Uvigerina curticosta	18.03	−31.40 ± 0.037	0.10	*Grossman & Ku* (1986)
Uvigerina flintii	18.03	−31.71 ± 0.066	0.13	*Grossman & Ku* (1986)
Uvigerina peregrina	18.03	−31.73 ± 0.039	0.20	*Grossman & Ku* (1986) *Marchitto et al.* (2014)
Genus:				
Bulimina	18.03	−31.95 ± 0.012	0.14	*Barras et al.* (2010) *McCorkle et al.* (2008)
Cibicidoides	18.03	−32.23 ± 0.013	0.11	*Keigwin* (1998) *Marchitto et al.* (2014)
Globigerina	18.03	−32.47 ± 0.031	0.21	*Bemis et al.* (1998) fig 1c *Mulitza et al.* (2003) *Spero & Lea* (1996)
Globigerinoides	18.03	−32.75 ± 0.022	0.21	*Mulitza et al.* (2003)
Globorotalia	18.03	−32.11 ± 0.038	0.25	*Lončarić et al.* (2006)
Hoeglundina	18.03	−31.06 ± 0.026	0.27	*Grossman & Ku* (1986) *Marchitto et al.* (2014)
Neogloboquadrina	18.03	−32.32 ± 0.045	0.31	*Mulitza et al.* (2003)
Orbulina	18.03	−31.95 ± 0.041	0.18	*Bemis et al.* (1998) fig 1a *Spero & Lea* (1993)
Planulina	18.03	−32.29 ± 0.036	0.16	*Marchitto et al.* (2014)
Rosalina	18.03	−32.18 ± 0.025	0.12	*McCorkle et al.* (2008)
Trilobatus	18.03	−32.67 ± 0.027	0.22	*Mulitza et al.* (2003)
Uvigerina	18.03	−31.73 ± 0.025	0.21	*Grossman & Ku* (1986) *Keigwin* (1998) *Marchitto et al.* (2014)
Other:				
Cibicidoides + Planulina	18.03	−32.24 ± 0.013	0.13	see above
all planktics	18.03	−32.49 ± 0.020	0.35	see above

Table 4 — Best-fit relationships between $^{18}\alpha$ and calcification temperature for different foraminifer species or genera, with $1000 \cdot \ln(^{18}\alpha) = A/T + B$. Species-specific offsets (B) are estimated by least-squares regression of the data shown in fig. 3. SE is the standard error of the best-fit values of B, with observation error estimates based on the scatter (RMSWD) in each data set. SD is the standard deviation of all observations for teach population. Best-fit B values and observation scatter are also shown in fig. 5.

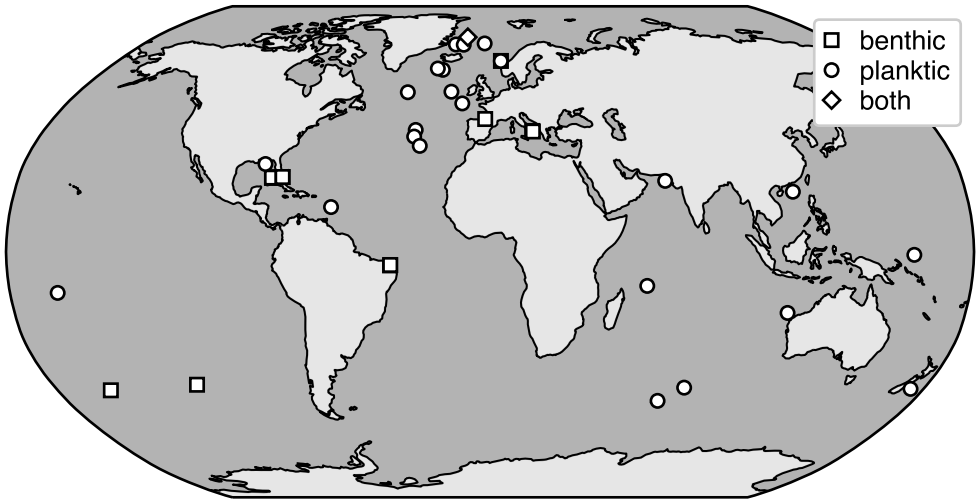

Figure 1 — Locations of the core-top sites listed in table 1.

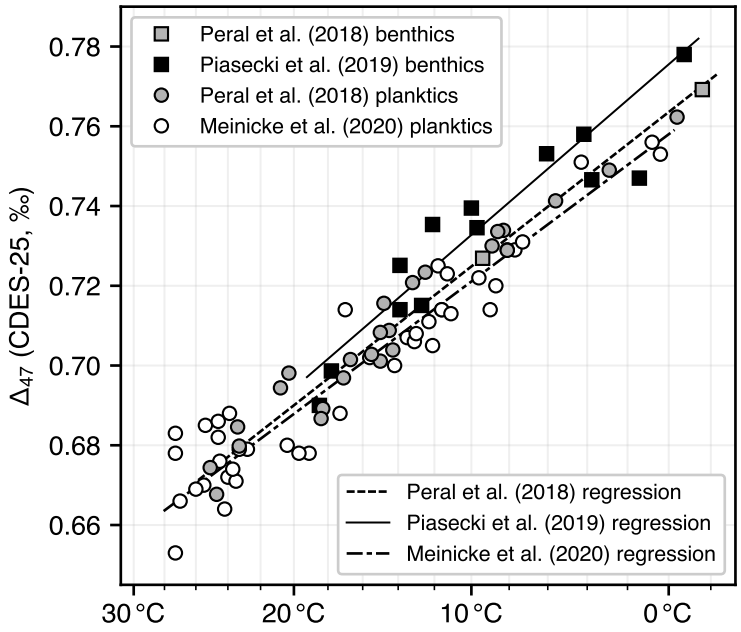

Figure 2 — Foraminifer calibration data sets as originally published. Different studies used different methods to estimate calcification temperatures (see section 2.3.1). Δ_{47} values are standardized using the same set of reference materials but correspond to the "historical" CDES scale (*Dennis et al.*, 2011).

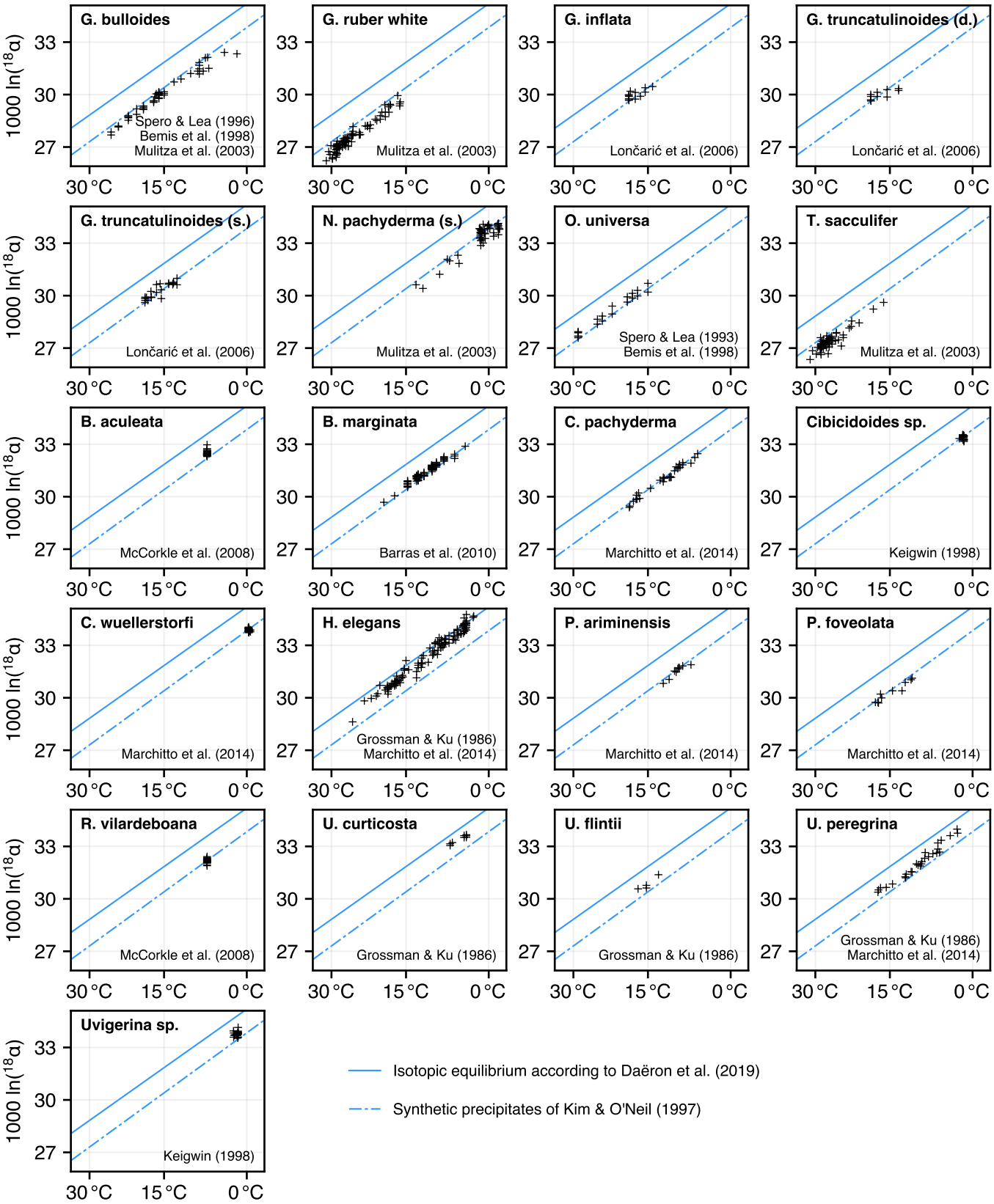

Figure 3 — Constraints linking $^{18}\alpha$ to calcification temperatures for species listed in table 2. Although these fractionation relationships differ between species, their temperature sensitivities remain indistinguishable from that for inorganic calcite (blue lines). All temperatures observations are from the original studies.

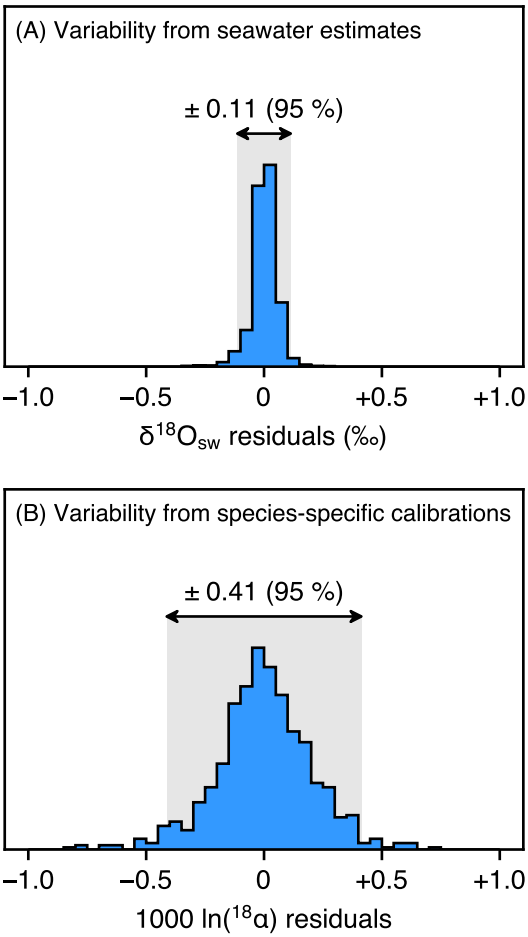

Figure 4 — Sources of uncertainty affecting the use of oxygen-18 thermometry to constrain planktic foraminifer calcification temperatures. (A) Overall residuals for the depth- and month-integrated $\delta^{18}O_{sw}$ values used to estimate seawater oxygen-18 composition for each planktic foraminifer sample. (B) Overall residuals for the species-specific oxygen-18 relationships listed in table 4, based on all studies shown in fig. 3.

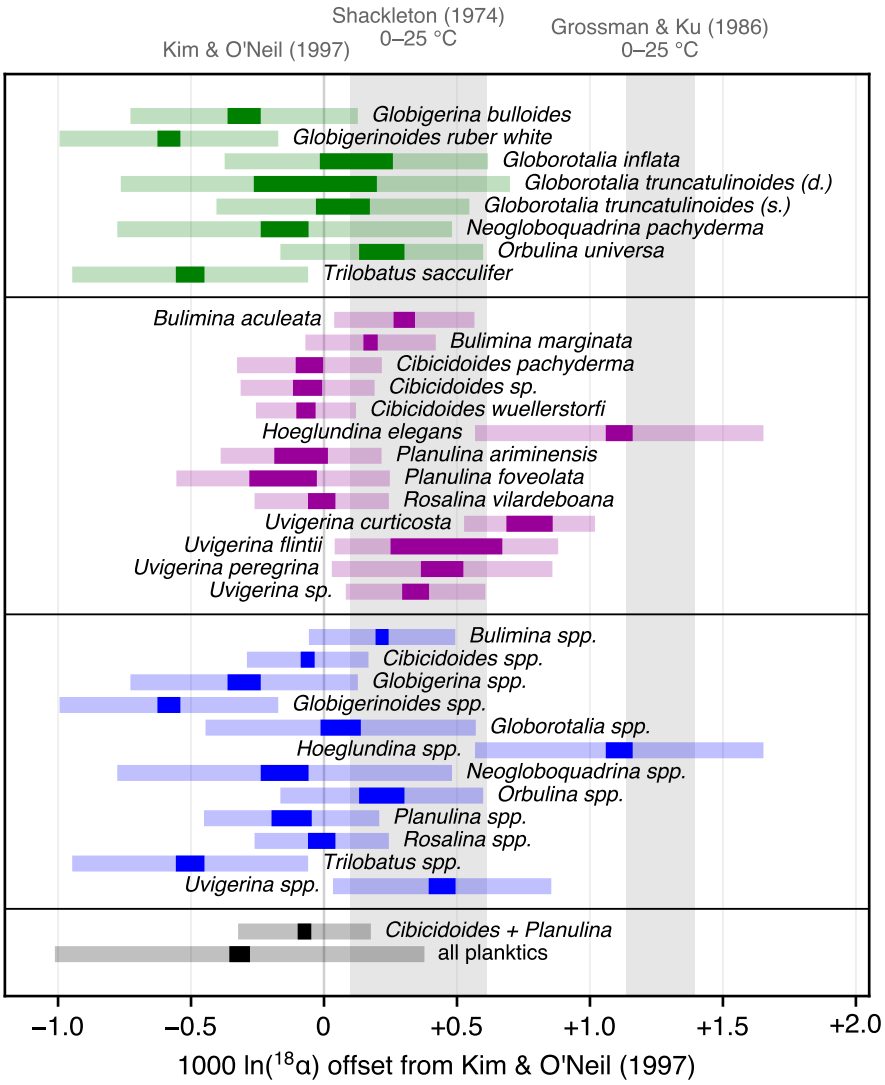

Figure 5 — Graphical summary of best-fit *B* values listed in table 4 for planktic (green) and benthic (purple) species, or by genus (blue). Dark bars correspond to ±95 % limits based on the SE of best-fit values; light bars represent the total spread of observations. Grey shaded regions correspond to the calcite calibrations of *Kim & O'Neil* (1997) and *Shackleton* (1974) in the range of 0–25 °C. Also shown is the aragonite calibration of *Grossman & Ku* (1986) which potentially applies to *H. elegans*, the only aragonitic species shown here.

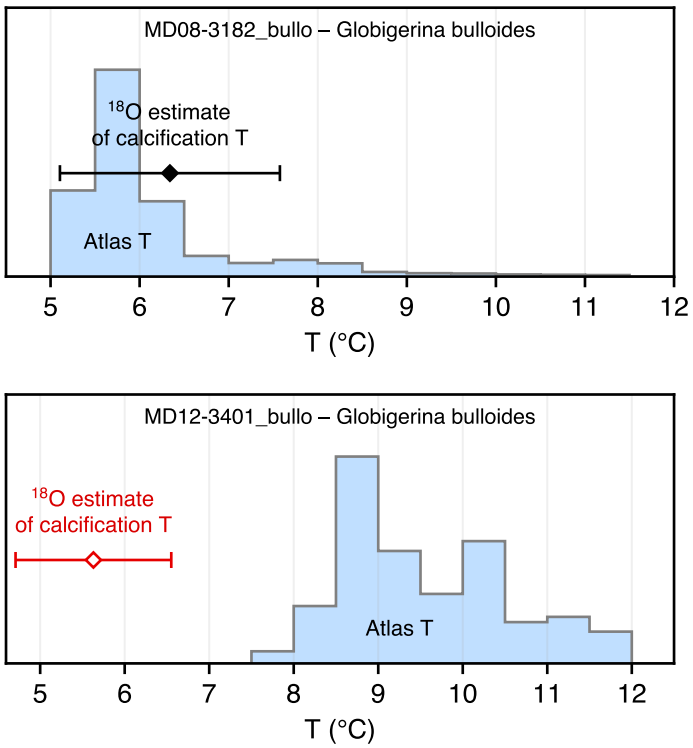

Figure 6 — Planktic samples are categorized as *concordant* (top panel) or *discordant* (bottom panel) depending on whether the oxygen-18 estimate of their calcification temperature (red or black 95 % error bar) overlaps with the seasonal distribution of temperatures (blue histogram) in the assumed calcification depth range for that species.

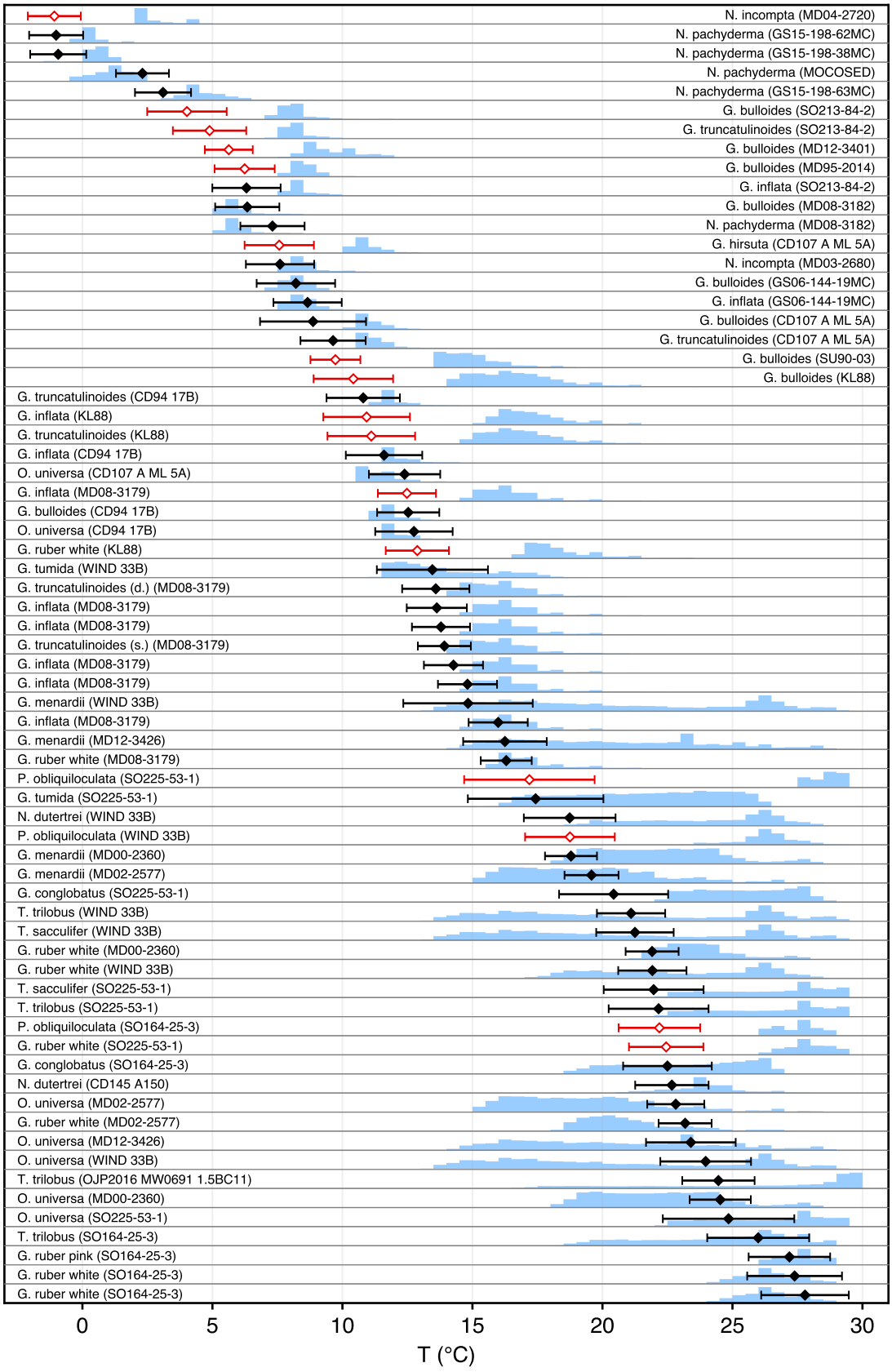

Figure 7 — Comparison, for each planktic sample from *Peral et al.* (2018) and *Meinicke et al.* (2020), between oxygen-18 estimates of calcification temperatures (95 % error bars) and year-long distribution (blue histograms) of monthly mean temperatures over the assumed living depth interval. T_{18} error bars for concordant and discordant samples are shown in black or red, respectively.

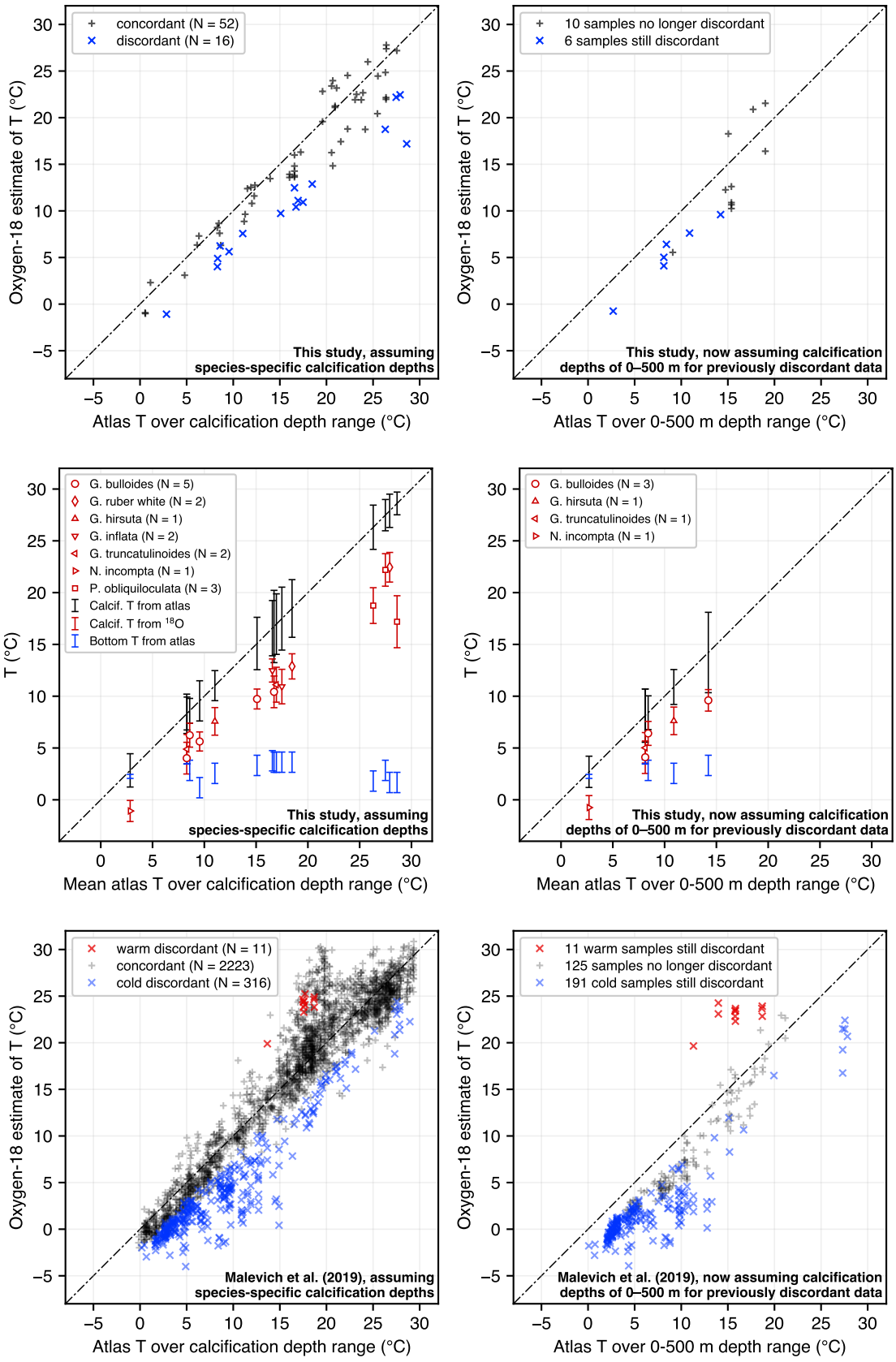

Figure 8 — Distribution of discordant samples in our clumped-isotope data set (*Peral et al.*, 2018; *Meinicke et al.*, 2020, top two rows) and in a much larger compilation of Holocene core tops (*Malevich et al.*, 2019, bottom row). Top row: T_{18} vs atlas temperatures over assumed living depth range (left panel) or over 0–500 m (right panel) for the clumped-isotope data set. Center row: Comparison of T_{18} with local bottom ocean temperatures and with atlas temperatures over assumed living depth range (left panel) or over 0–500 m (right panel) for the clumped-isotope data set Bottom row: T_{18} vs atlas temperatures over assumed living depth range (left panel) or over 0–500 m (right panel) for the *Malevich et al.* data set. Right panel in each row only shows previously discordant samples.

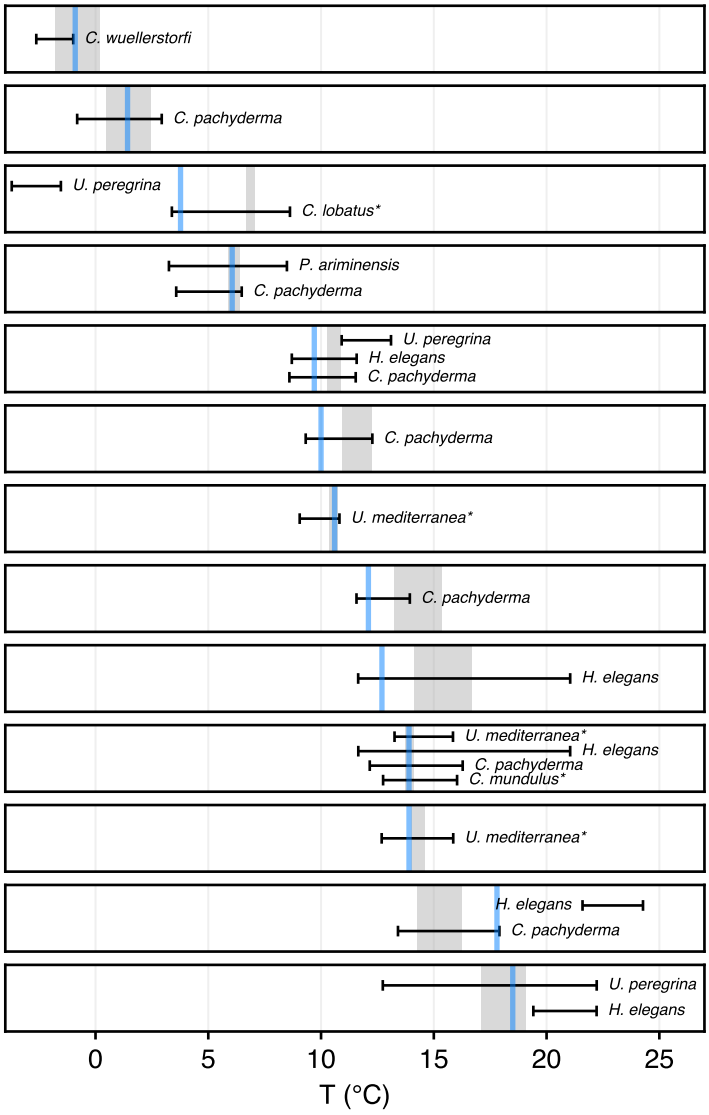

Figure 9 — Comparison, for each benthic sample from *Peral et al.* (2018) and *Piasecki et al.* (2019), between oxygen-18 estimates of calcification temperatures (95 % error bars), bottom mean annual temperatures (95 % grey shading), and originally reported calcification temperatures (blue lines). Species listed with asterisks are those without direct observations constraining $^{18}\alpha$.

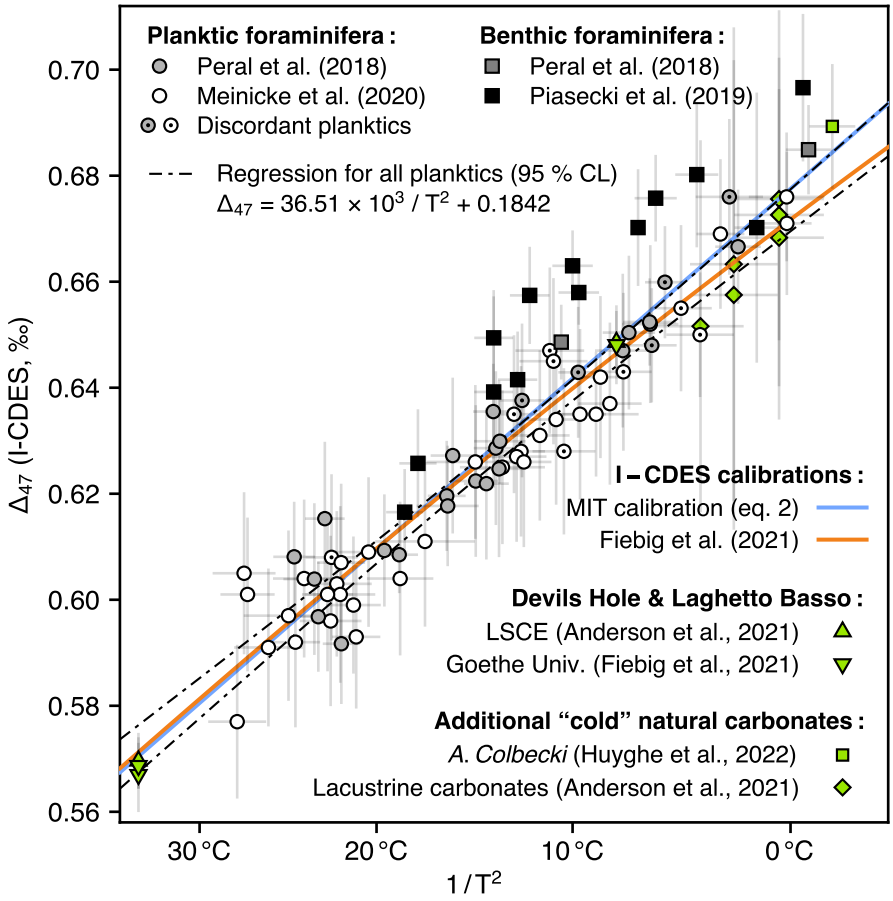

Figure 10 — Foraminiferal Δ_{47} as a function of calcification temperature as documented by the three studies considered here. As discussed in text, the three planktic samples with coldest T_{18} values were assigned calcification temperatures based on the narrow range of monthly WOA23 temperatures between 0 and 1500 m depth (section 3.2.2), and three discordant planktic samples of species *P. obliquiloculata* were excluded due to poorly constrained $^{18}\alpha$ values (section 3.4.3). Benthic calcification temperatures are from original publications, where available, or otherwise redetermined from WOA23. The MIT calibration shown here is recalculated based on the full results listed in the supplemental table S1 of *Anderson et al.* (2021), in order to avoid including the foraminifer observations re-assessed here (see section 3.4.1). The low-temperature natural carbonates mentioned in section 3.5 are shown as green squares and diamonds.

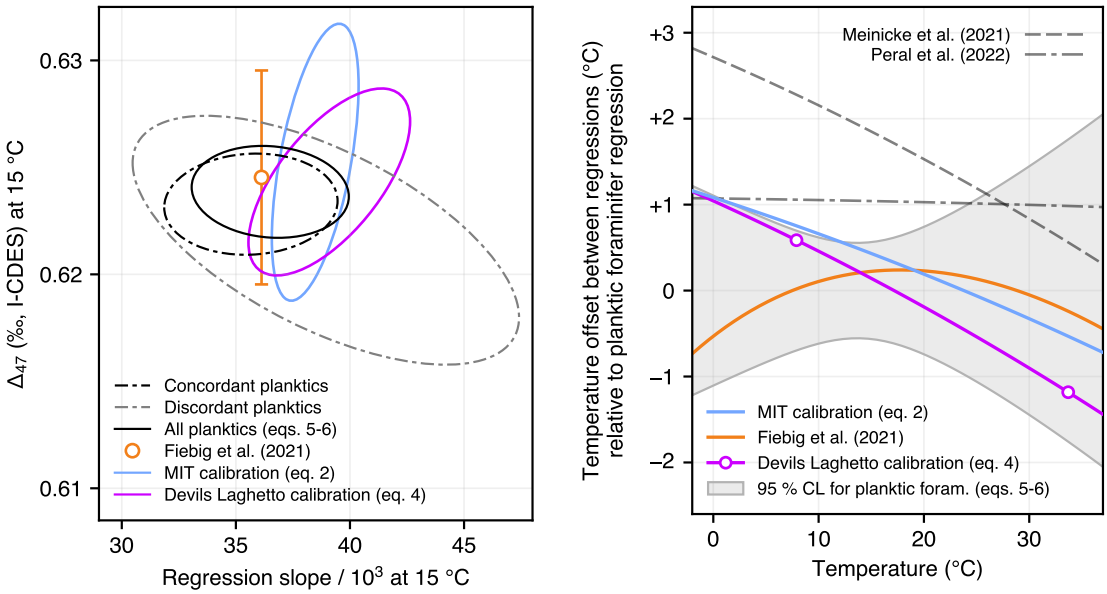

Figure 11 — Left panel: 95 % confidence ellipses for the regression slope and Δ_{47} value at 15 °C for various regressions. The "Devils Laghetto" regression (purple ellipse, eq. 4) only includes slow-growing calcite believed to achieve quasi-equilibrium Δ_{47} values, based on the independent measurements (green triangles in fig. 10) reported by *Anderson et al.* (2021) and *Fiebig et al.* (2021). Due to the use of a quadratic formula by *Fiebig et al.* (2021), only their local slope and 95 % confidence region for Δ_{47} at 15 °C are shown here. Right panel: difference in reconstructed temperatures using various calibrations. 95 % confidence bounds (not shown here) for the MIT and *Fiebig et al.* calibrations are both around ± 1.8 °C; those for the Devils Laghetto regression are about ± 1.2 °C.

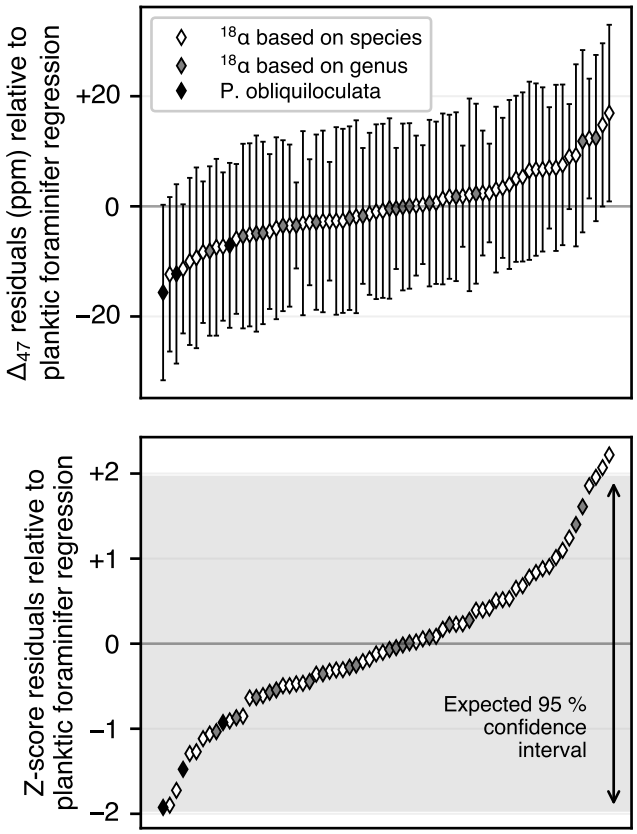

Figure 12 — Regression residuals for the planktic samples from *Peral et al.* (2018) and *Meinicke et al.* (2020). Error bars in top panel are with 95 % confidence limits from combined uncertainties in Δ_{47} and calcification temperatures. Z-scores in bottom panel are computed based on these same error bars.

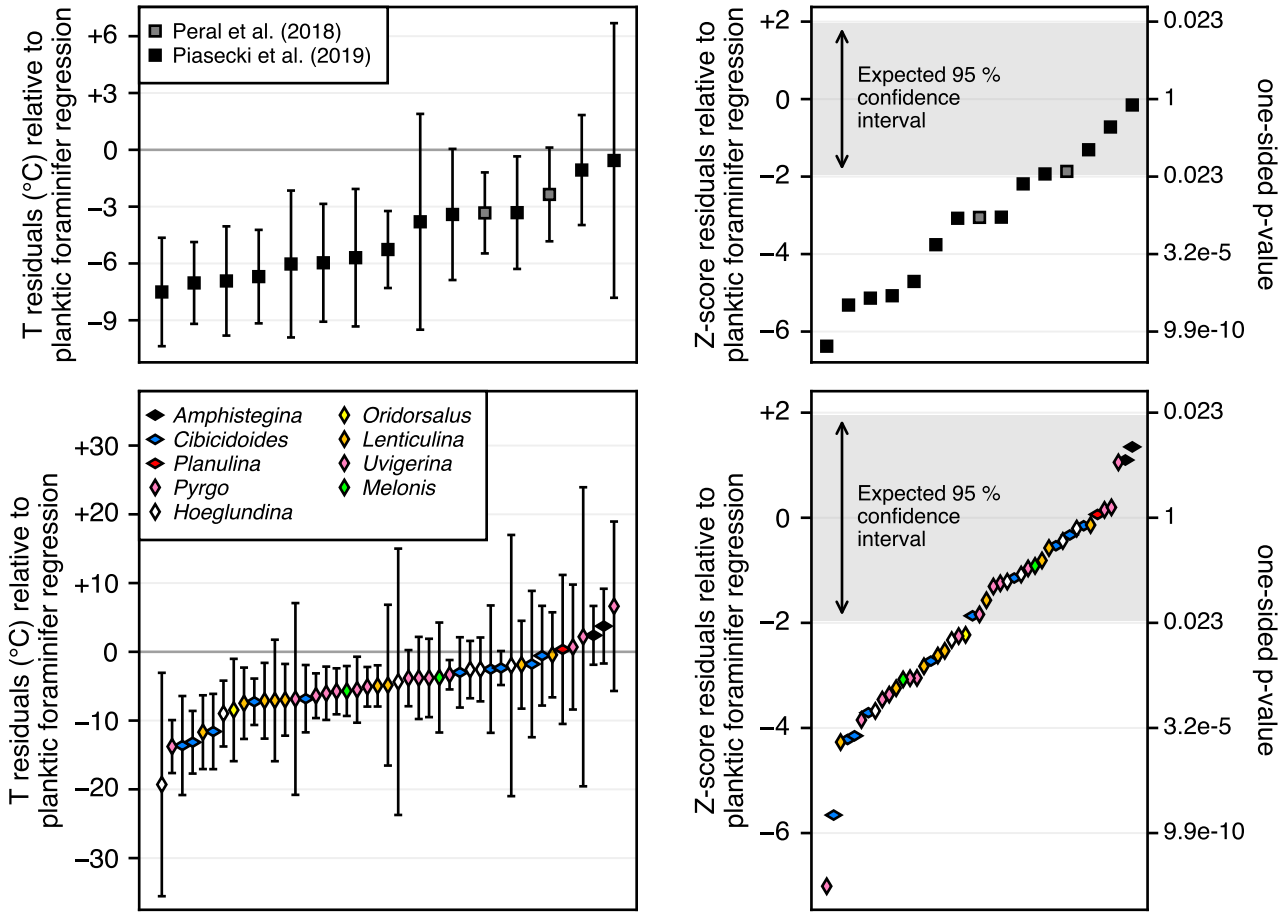

Figure 13 — Temperature residuals (left panels) and corresponding Z-scores (right panels) for benthic samples from *Peral et al.* (2018) and *Piasecki et al.* (2019), relative to the planktic regression of eq. 5. Top row: results averaged by core top. Bottom row: results averaged by species at each core top. Vertical and horizontal diamonds represent infaunal and epifaunal species, respectively. Colored markers correspond to different genera. The right axis in each of right panels indicates the p-values corresponding to Z-scores for a Gaussian distribution.

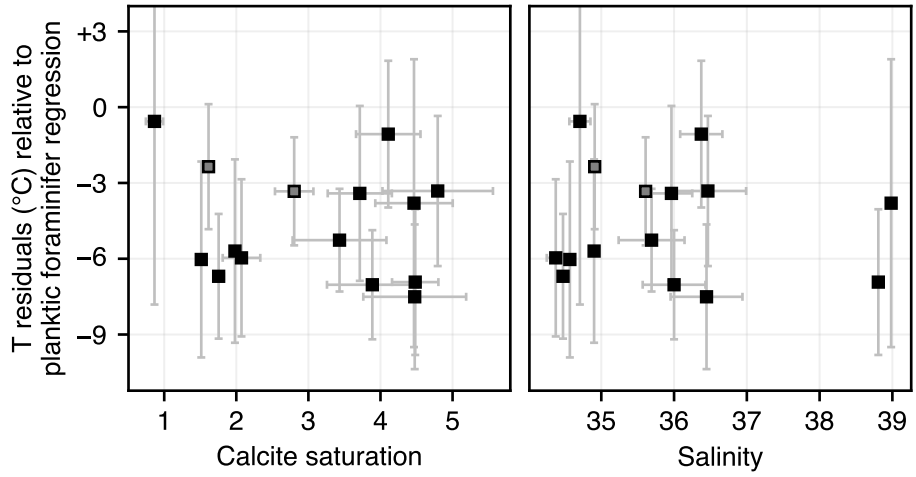

Figure 14 — The benthic residuals of fig. 13 are not obviously correlated with seawater chemistry. Calcite saturation and salinity were estimated from GLODAPv2 (*Lauvset et al.*, 2016).

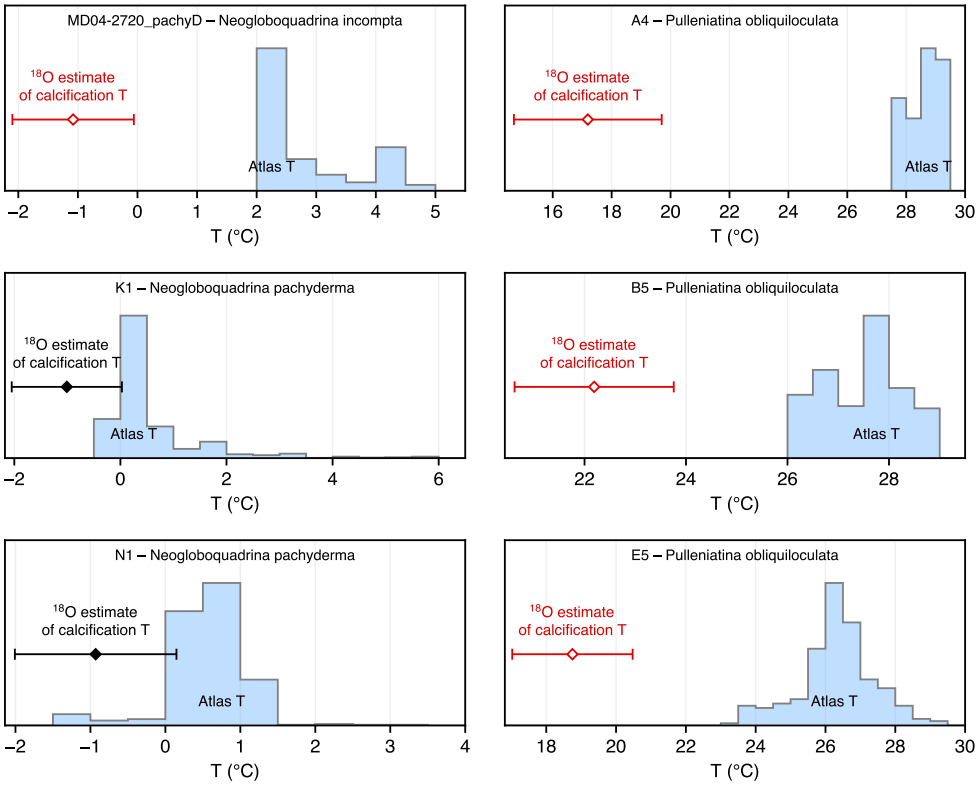

Figure 15 — Comparison between oxygen-18 estimates of calcification temperatures (95 % error bars) and year-long distribution (blue histograms) of monthly mean temperatures over the assumed living depth interval for the three coldest planktic samples (left column, see section 3.2.2) and the *P. obliquiloculata* samples (right column, see section 3.4.3).

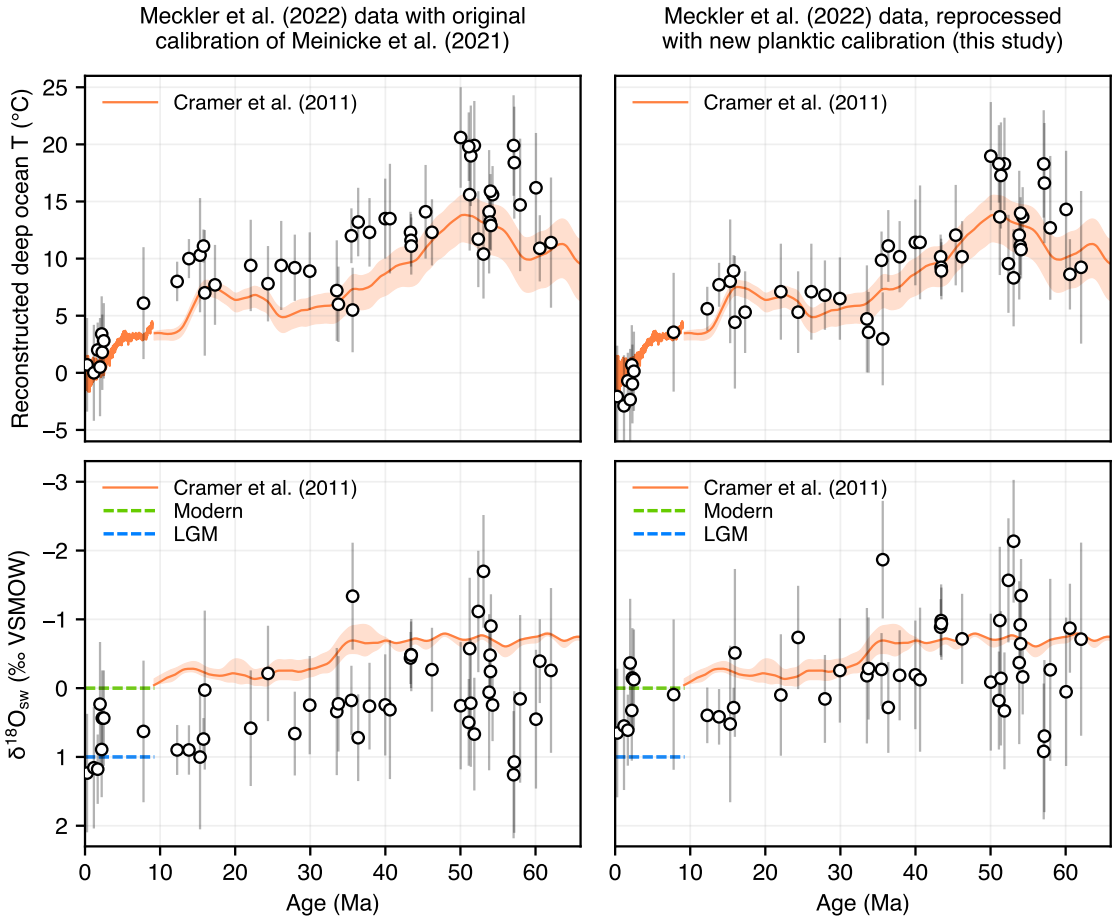

Figure 16 — Left column: original reconstructions of Cenozoic deep ocean temperatures and $\delta^{18}O_{sw}$ by *Meckler et al.* (2022) using the Δ_{47} calibration of *Meinicke et al.* (2021). Note the conspicuous offset between the Δ_{47} paleotemperatures (round markers, with 95 % confidence intervals) and reconstructions based on benthic foraminifer $\delta^{18}O_c$ (orange lines with shaded confidence limits). Right column: using this study's planktic regression instead (eq. 5) largely reconciles these results with the $\delta^{18}O_c$ record (see figs. 17 and S5 for corresponding plots of the offset between T_{47} and T_{18}, and figs. S6–S8 using the different I-CDES calibrations). When using the planktic calibration, the average of $\delta^{18}O_{sw}$ before 45 Ma is -0.60 ± 0.16 ‰ (2SE) for the Δ_{47} samples, to be compared with an average value of -0.73 ± 0.4 ‰ for the same period of the *Cramer et al.* reconstruction.

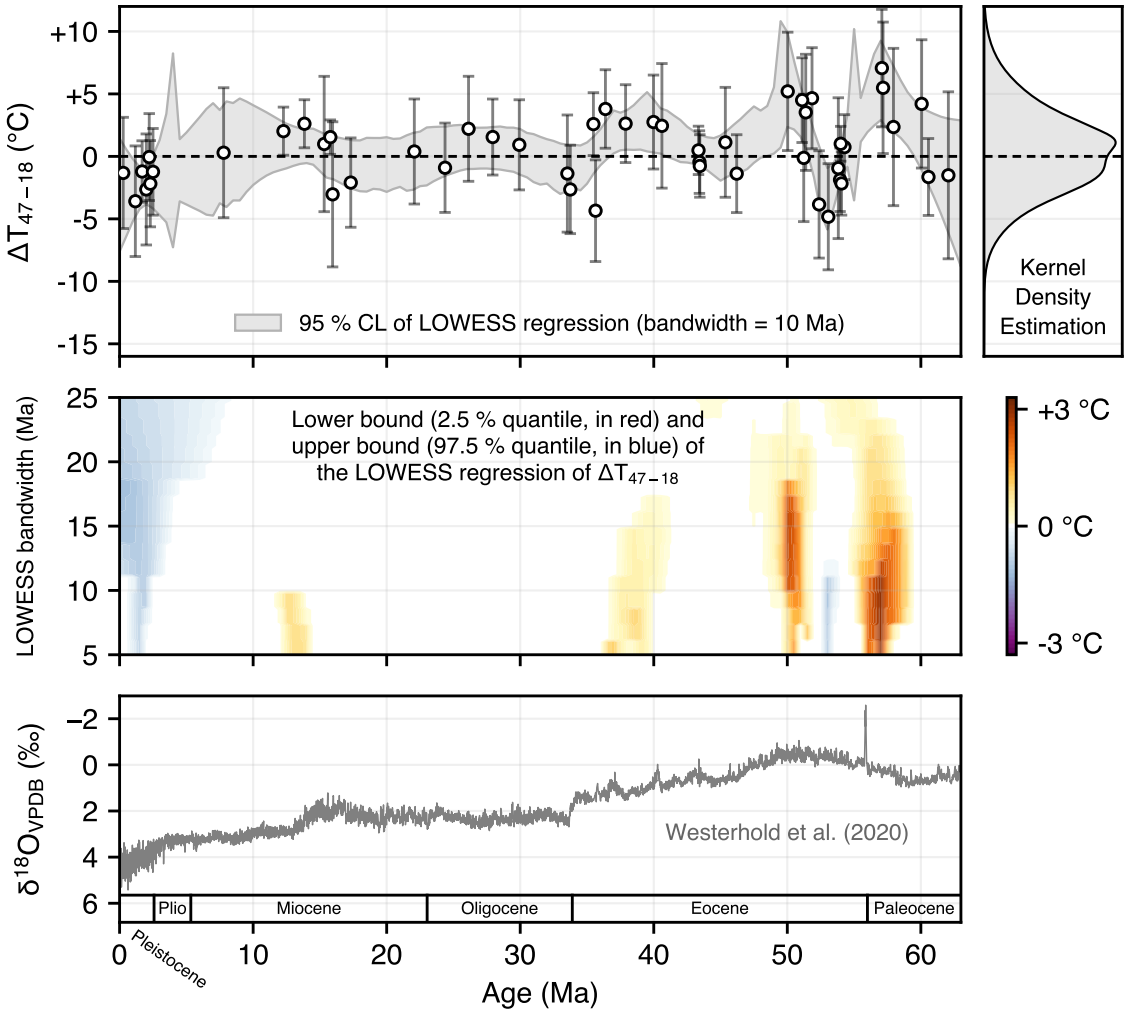

Figure 17 — Top left: plot of $\Delta T_{47\text{-}18}$, defined as the difference between the benthic T_{47} values of *Meckler et al.* (2022), reprocessed using this study's planktic regression (eq. 5), and the corresponding $\delta^{18}O_c$-derived T_{18} record from *Cramer et al.* (2011). Vertical error bars account for estimated analytical and calibration errors on Δ_{47} as well as the originally reported T_{18} uncertainties. Green shaded area is the central 95 % confidence band for a LOWESS regression of $\Delta T_{47\text{-}18}$ with a bandwidth equal to 10 Ma. Top right: kernel density estimation (KDE) for the whole (unsmoothed) data set, showing that the long-term average of $\Delta T_{47\text{-}18}$ is close to zero. Center panel: white areas correspond to periods when $\Delta T_{47\text{-}18}$ does not significantly differ from zero, and shaded areas to periods when T_{47} is significantly warmer (in red) or colder (in blue) than T_{18} at the 95 % confidence level, with color density corresponding to the 2.5 % and 97.5 % quantiles, respectively, of ($T_{47} - T_{18}$). Note that color densities conservatively denote the *minimum* level of mismatch (at 95 % confidence); *average* values of smoothed $\Delta T_{47\text{-}18}$ are further away from zero. Bottom panel: smoothed benthic $\delta^{18}O_c$ record of *Westerhold et al.* (2020).

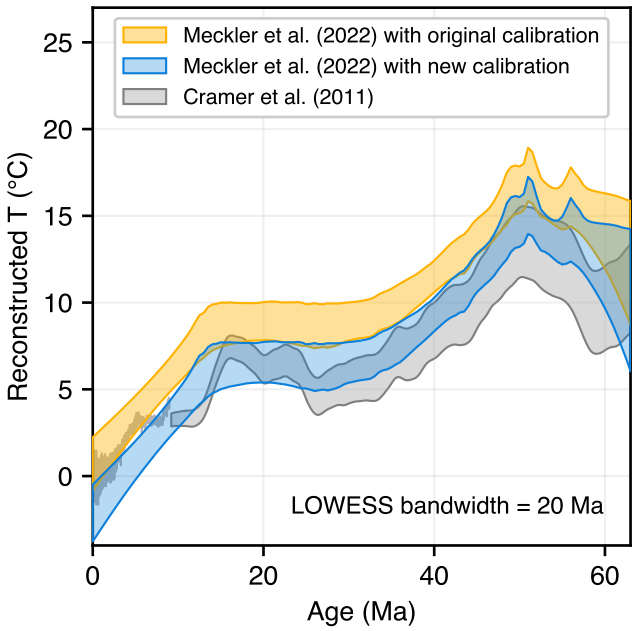

Figure 18 — Comparison of smoothed reconstructions of deep ocean temperature. In gray: 90 % confidence band of T_{18} reconstructed by *Cramer et al.* (2011). In yellow: 95 % confidence band of a LOWESS regression of the *Meckler et al.* (2022) data, converted to T_{47} using the *Meinicke et al.* (2021) calibration. In blue: 95 % confidence band of a LOWESS regression of the same data, but converted to T_{47} using our new planktic calibration (eq. 5). The LOWESS bandwidth was chosen arbitrarily to yield approximately the same width and level of detail as the *Cramer et al.* reconstruction. LOWESS 95 % confidence limits are estimated using a quasi-Monte Carlo simulation where we quasi-randomly generate 2^{13} versions of the T_{47} data set.

ACCEPTED FOR PUBLICATION IN *PALEOCEANOGRAPHY & PALEOCLIMATOLOGY* ON 2023-09-22

Revisiting oxygen-18 and clumped isotopes in planktic and benthic foraminifera

Supporting Information

M. Daëron* (1) W. R. Gray (1)

* daeron@lsce.ipsl.fr

(1) *Laboratoire des Sciences du Climat et de l'Environnement, LSCE/IPSL, CEA-CNRS-UVSQ, Université Paris-Saclay, Orme des Merisiers, 91191 Gif-sur-Yvette, France.*

- **Figure S1:** Example of our bottom temperature determination procedure
- **Figure S2:** Comparison of T_{18} versus atlas temperatures for depths down to 500 m
- **Figure S3:** Comparison of T_{18} versus atlas temperatures for depths down to 1500 m
- **Figure S4:** Differences in $\delta^{13}C$ between discordant and concordant planktic samples
- **Figure S5:** Offsets between Δ_{47}-derived and $\delta^{18}O$-derived estimates of deep ocean temperatures over the Cenezoic, based on reconstructions by *Cramer et al.* (2011) and measurements by *Meckler et al.* (2022), when using two different Δ_{47} calibrations.
- **Figure S6:** A different version of fig. 16, using the Devils Laghetto calibration
- **Figure S7:** A different version of fig. 16, using the MIT calibration
- **Figure S8:** A different version of fig. 16, using the *Fiebig et al.* (2021) calibration

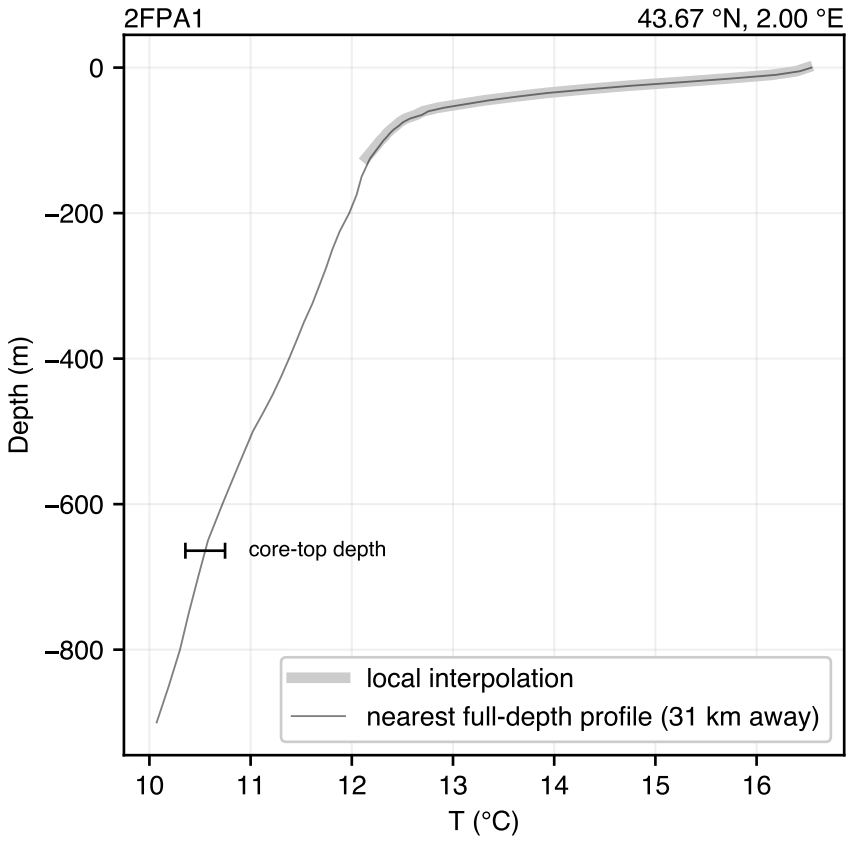

Figure S1 — We estimate bottom seawater temperature (black error bars corresponding to 95 % confidence limits) at each core top by using the nearest neighboring WOA23 grid node with a temperature profile reaching sufficient depth. We check the consistency between the temperature profile interpolated at the latitude and longitude of the core (thick grey line) and the nearest-neighbor temperatures (thin line) by visual inspection of the two superimposed profiles

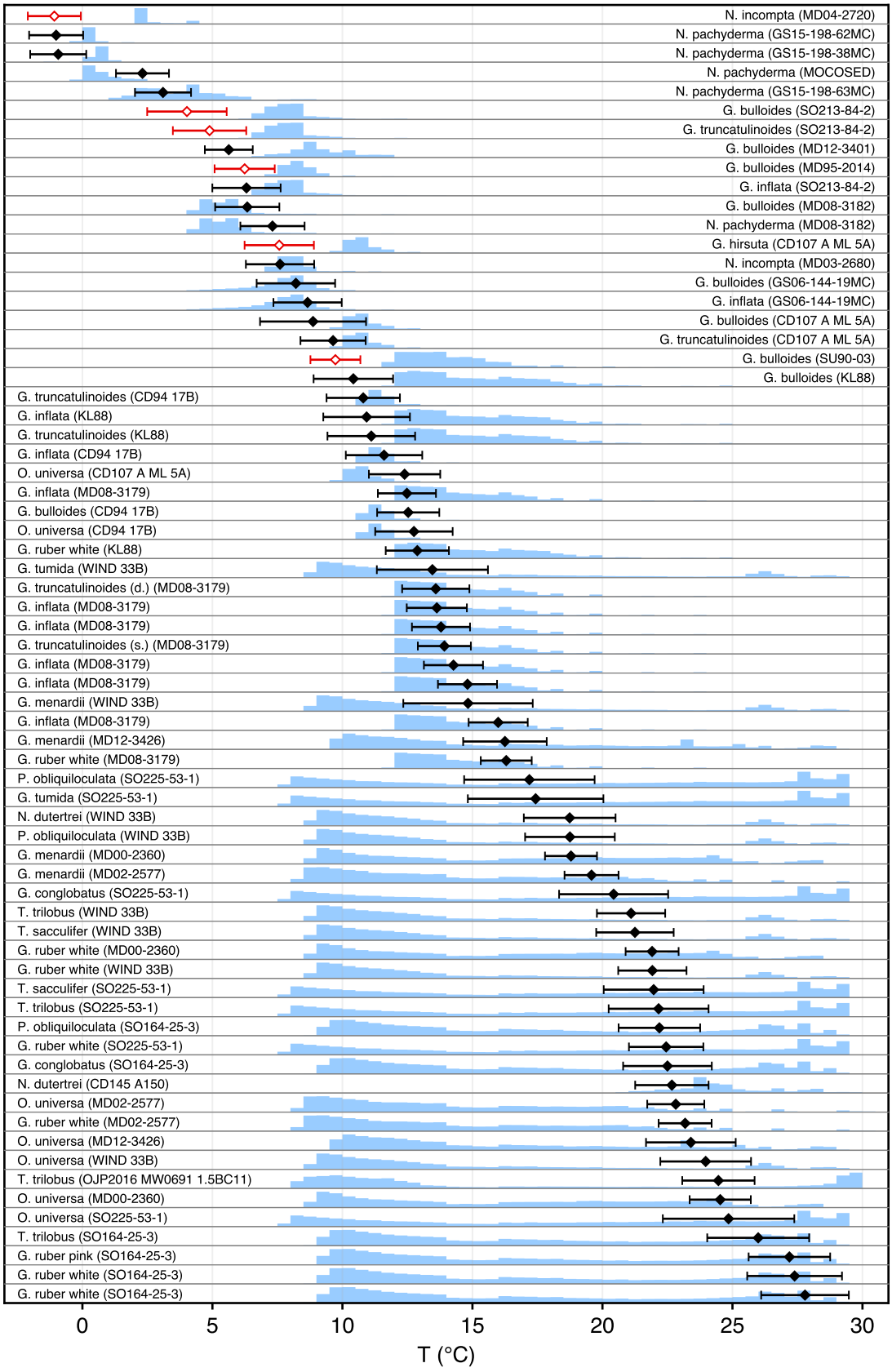

Figure S2 — Comparison, for each planktic sample from *Peral et al.* (2018) and *Meinicke et al.* (2020), between oxygen-18 estimates of calcification temperatures (95 % error bars) and year-long distribution (blue histograms) of monthly mean temperatures over depths of 0–500 m. T_{18} error bars for concordant and discordant samples are shown in black or red, respectively.

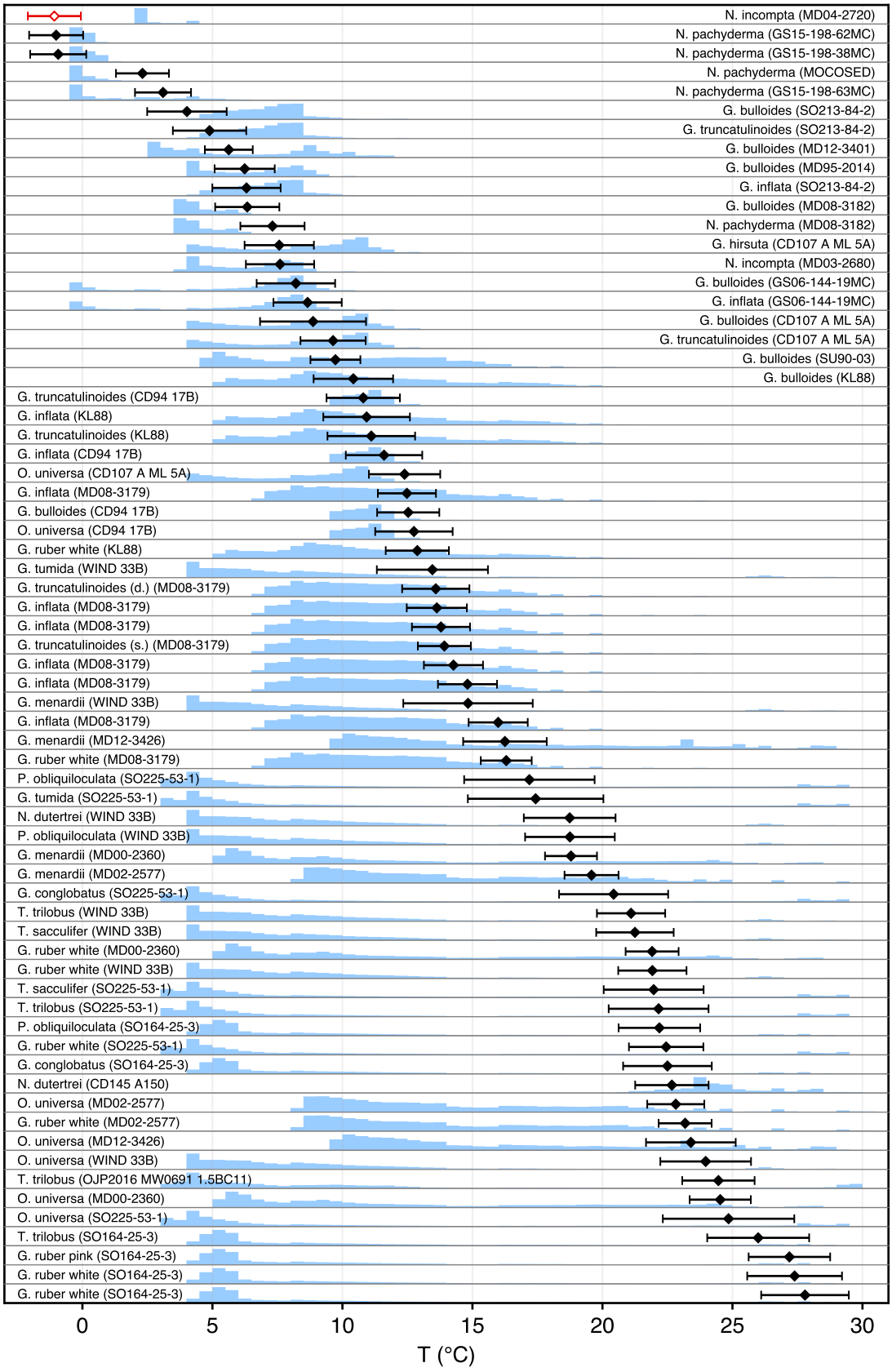

Figure S3 — Comparison, for each planktic sample from *Peral et al.* (2018) and *Meinicke et al.* (2020), between oxygen-18 estimates of calcification temperatures (95 % error bars) and year-long distribution (blue histograms) of monthly mean temperatures over depths of 0–1500 m. T_{18} error bars for concordant and discordant samples are shown in black or red, respectively.

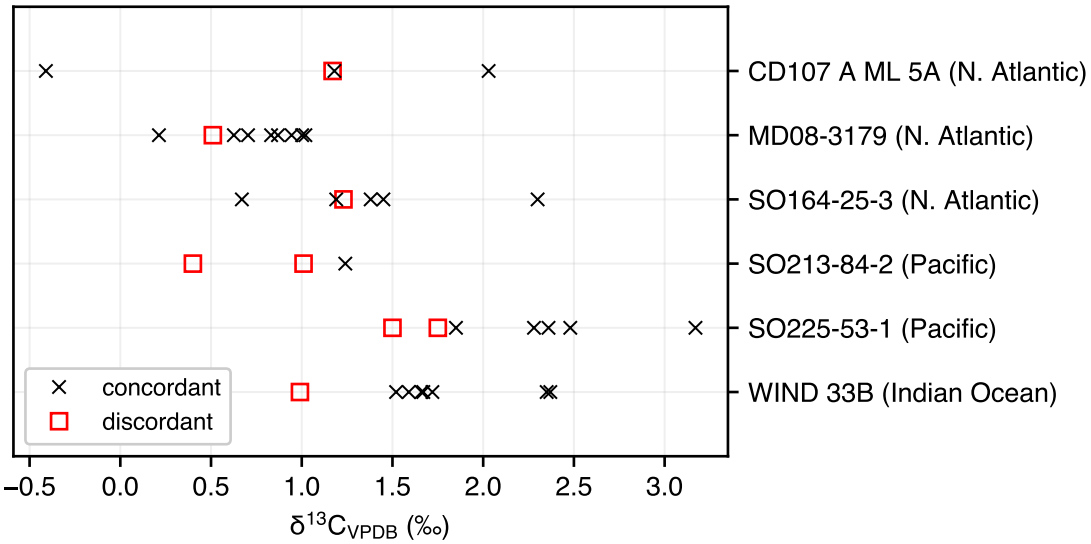

Figure S4 — Differences in $\delta^{13}C$ between discordant and concordant planktic samples from the same site: in ocean basins with strong vertical $\delta^{13}C$ gradients (Indian and Pacific oceans), discordant samples have lower $\delta^{13}C$ values than concordant ones from the same site, whereas discordants from the North Atlantic ocean, where the gradient is much weaker, have $\delta^{13}C$ values indistinguishable from concordant samples from the same site, suggesting that discordant samples may reflect deeper calcification than expected based on typical living depths.

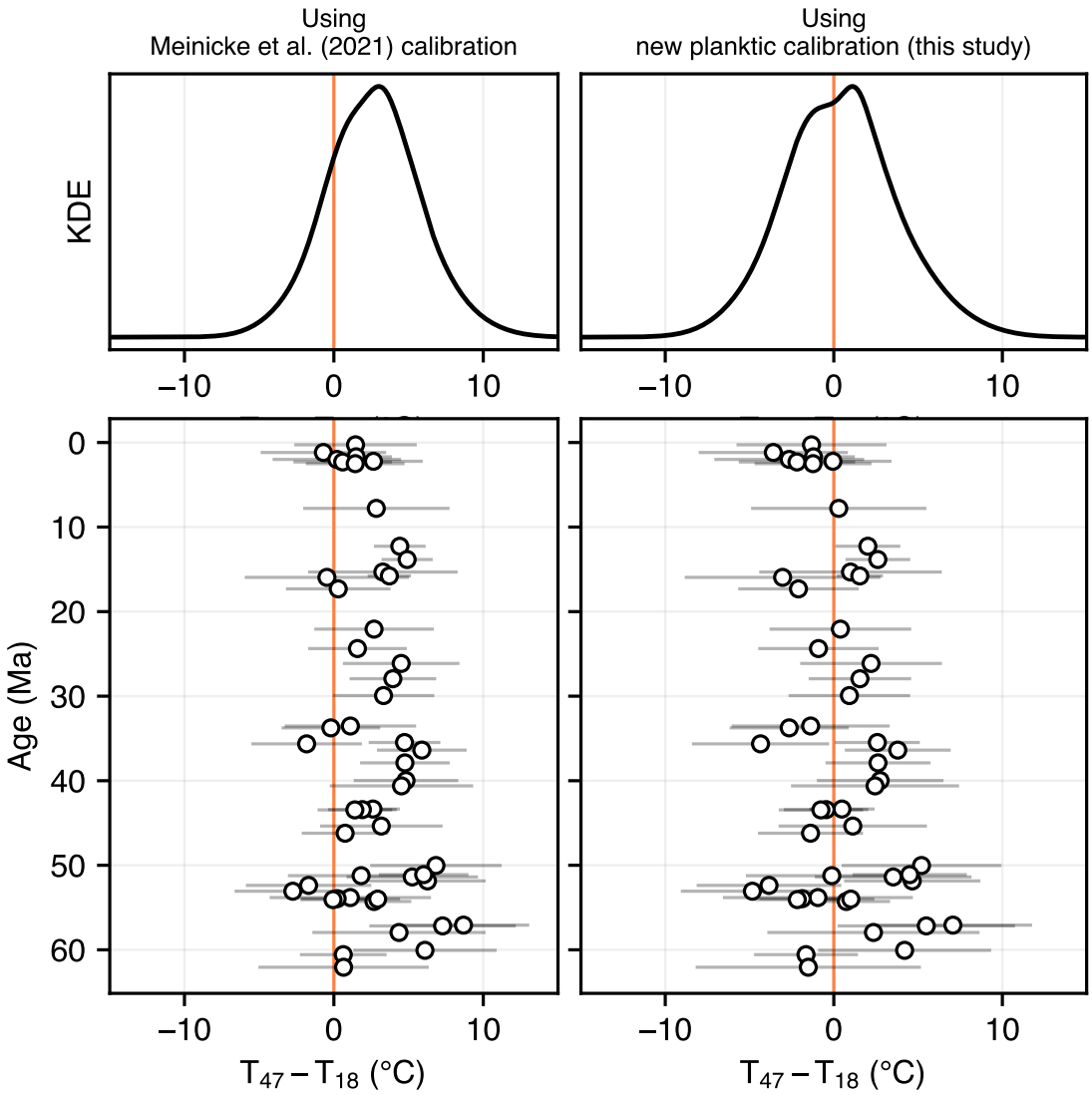

Figure S5 — Left column: offset between T_{18} (based on *Cramer et al.* (2011) and T_{47} (based on the *Meinicke et al.* (2021) calibration as in the original publication) for the Cenozoic deep ocean temperature reconstruction of *Meckler et al.* (2022). Error bars correspond to 95 % confidence limits of Δ_{47} reconstructions, and the corresponding overall kernel density estimation (KDE) is unambiguously offset from zero by 2–3 °C. Right column: the same comparison, but with T_{47} based on this study's planktic Δ_{47} regression (eq. 5), resulting in a zero-centered KDE.

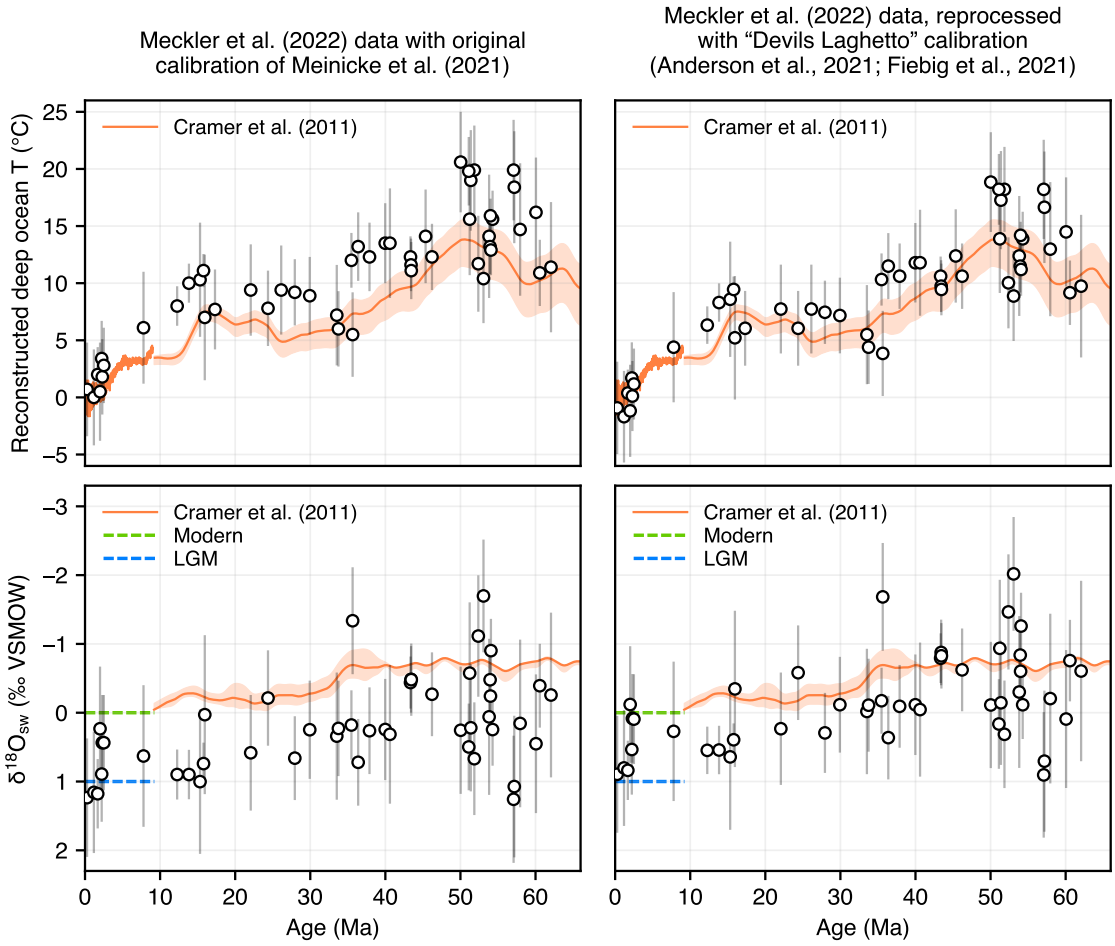

Figure S6 — A different version of fig. 16, using the Devils Laghetto calibration (eq. 4).

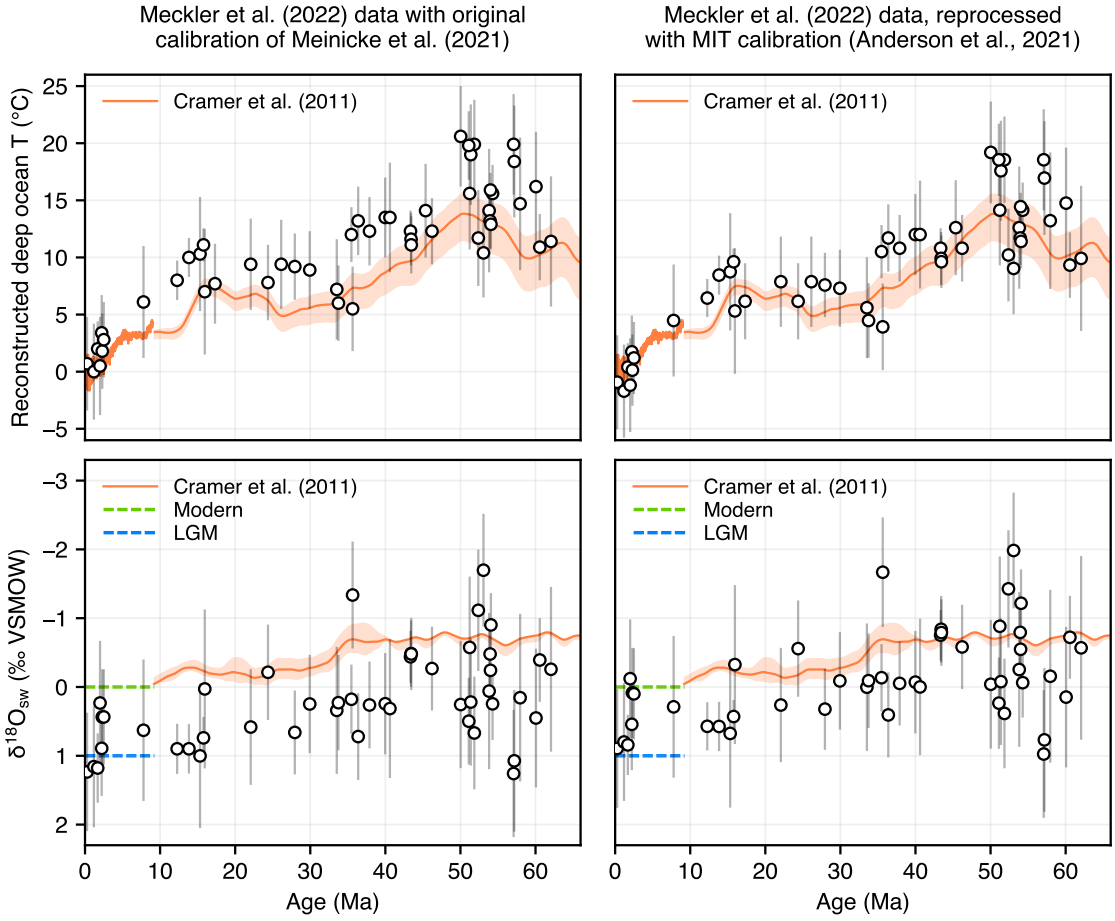

Figure S7 — A different version of fig. 16, using the MIT calibration (eq. 2). As stated in section 3.4.1, this calibration only includes the measurements performed at MIT as originally reported by *Anderson et al.* (2021). Note that fig. S3 of *Meckler et al.* (2022) uses instead the composite calibration equation published by *Anderson et al.*, which includes the whole *Peral et al.* (2018) data set (with calcification temperatures based on *Kim & O'Neil*, 1997) as well as the *Meinicke et al.* (2021) data (with temperatures based on *Shackleton*, 1974).

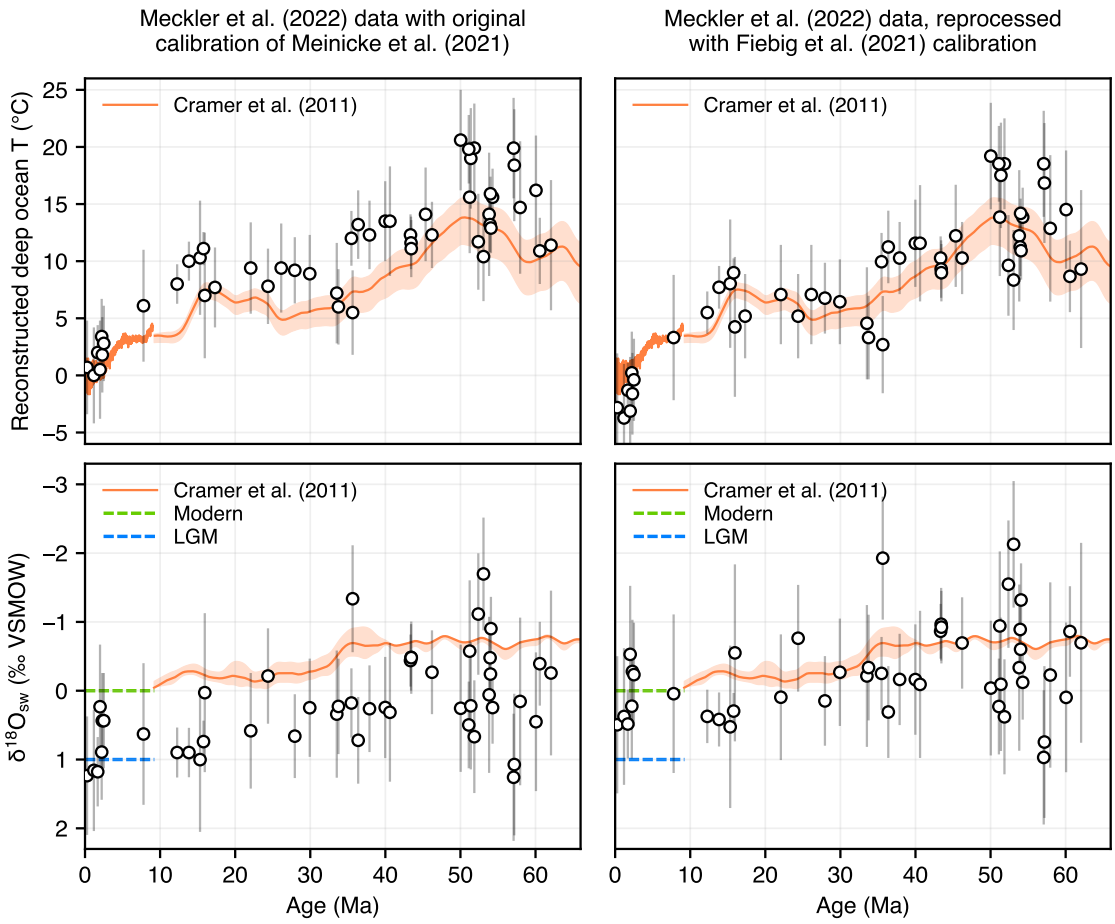

Figure S8 — A different version of fig. 16, using the *Fiebig et al.* (2021) calibration.